

Modernizing full posterior inference for surrogate modeling of categorical-output simulation experiments

Andrew Cooper*

Annie S. Booth[†]

Robert B. Gramacy[†]

January 28, 2025

Abstract

Gaussian processes (GPs) are powerful tools for nonlinear classification in which latent GPs are combined with link functions. But GPs do not scale well to large training data. This is compounded for classification where the latent GPs require Markov chain Monte Carlo integration. Consequently, fully Bayesian, sampling-based approaches had been largely abandoned. Instead, maximization-based alternatives, such as Laplace/variational inference (VI) combined with low rank approximations, are preferred. Though feasible for large training data sets, such schemes sacrifice uncertainty quantification and modeling fidelity, two aspects that are important to our work on surrogate modeling of computer simulation experiments. Here we are motivated by a large scale simulation of binary black hole (BBH) formation. We propose an alternative GP classification framework which uses elliptical slice sampling for Bayesian posterior integration and Vecchia approximation for computational thrift. We demonstrate superiority over VI-based alternatives for BBH simulations and other benchmark classification problems. We then extend our setup to warped inputs for “deep” nonstationary classification.

Keywords: Gaussian process, emulation, categorical data, Vecchia approximation, black hole simulation, elliptical slice sampling, nonstationary

1 Introduction

Model-based simulations of real-world phenomena allow researchers to conduct experiments that are either too costly or infeasible to perform in field tests (Morris et al., 1993; Santner et al., 2018); however, even simulations can be too computationally intensive to repeatedly sample. Meta-modeling a simulator with a statistical replacement – or “surrogate” – trained on a collection of simulator runs (i.e., input-output pairs) enables estimation of simulator output for unobserved inputs at a significantly reduced computational cost (Gramacy, 2020). An effective surrogate is able to capture the important features of a simulator’s response surface, while providing appropriate uncertainty quantification (UQ) at locations where training data is lacking. This can be crucial to many otherwise simulation-intensive downstream tasks such as computer model calibration (Kennedy and O’Hagan, 2001), input sensitivity analysis (Marrel et al., 2009), and active learning or Bayesian optimization (Jones et al., 1998).

One popular surrogate is a Gaussian process (GP; see, e.g., Rasmussen and Williams, 2006), which models the response as multivariate normal (MVN) with a covariance based on pairwise distances between inputs. GPs can flexibly capture nonlinear dynamics within a Bayesian framework, thereby providing predictive mean and variance with intuitive and well-calibrated UQ. Training a GP and evaluating its predictive equations involves decomposing covariance matrices, requiring flops that are cubic in the number of observations, n . This $\mathcal{O}(n^3)$ computational bottleneck can limit GP surrogates to small-to-medium sized simulation campaigns, e.g., $n \ll 10,000$.

*Corresponding author: Department of Statistics, Virginia Tech, ahcooper@vt.edu

[†]Department of Statistics, Virginia Tech

Our work is motivated by a large simulation campaign studying binary black holes (BBHs; [Lin et al., 2021](#); [Yazdi et al., 2024](#)) that can form when two massive celestial objects collide. The simulator estimates the “chirp mass” of the resulting BBH depending on eleven inputs describing the configuration of the system and celestial objects. BBH formation is rare; for most input configurations the simulator returns NA, meaning no BBH was formed. Here, we study the important sub-problem of predicting whether or not a BBH forms for a given input configuration. We propose tackling this problem with a GP surrogate, which presents two, intertwined challenges. The first is adapting GP surrogates to the classification problem while preserving modeling fidelity and UQ. The second is handling large data sizes, i.e., “big n .”

The typical setup for GP-based classification (GPC) analogues the way logistic regression extends linear regression, where an n -dimensional latent layer is estimated through an appropriate link function to a Bernoulli response (more on this in [Section 2.2](#)). This setup is intuitive but necessitates inference for at least n -many unknown quantities. Fully Bayesian GPC via Markov chain Monte Carlo (MCMC) posterior integration for all unknowns had long been abandoned, unless $n \ll 1,000$. Instead, practitioners preferred thriftier alternatives such as approximate variational inference (VI; [Damianou et al., 2016](#)), typically in tandem with inducing points (IPs; e.g., [Quiñonero et al., 2005](#)), for a low-rank matrix representation, and thus speedier matrix decompositions. But this recipe can lead to underwhelming predictive performance because the shortcuts are too severe ([Wu et al., 2022](#)). [Sauer et al. \(2022a\)](#) argue that in the context of computer simulation experiments (with real-valued outputs), VI with IPs also undercuts UQ. We see similarly poor behavior in our surrogate classification setting, which we will demonstrate empirically later.

To extend the toolkit for fully Bayesian GPC, we follow the roadmap provided by [Sauer et al. \(2022a\)](#), for “deep” GP regression, and adapt it to classification. This involves two ingredients: elliptical slice sampling (ESS; [Murray et al., 2010](#)) for high-dimensional posterior integration of Gaussian latent quantities and Vecchia approximation for sparse decomposition ([Vecchia, 1988](#); [Katzfuss and Guinness, 2021](#); [Datta et al., 2016](#)). ESS for Bayesian GPC is not new; in fact, that was the algorithm’s motivating application. Nevertheless, this approach is too cumbersome without additional approximation. Our novel insight is that Vecchia approximation is uniquely suited to ESS for GPC. We show that our Vecchia/ESS GPC provides more accurate predictions, with better UQ, compared to VI/IP and similar maximization-based alternatives, and provides similar performance to non-Vecchia-approximated ESS when possible, in smaller- n settings. We then take things one step further and show how the deep, warping-layer approach of [Sauer et al.](#), for regression, can be ported to classification for improved performance in nonstationary settings.

The paper is laid out as follows. [Section 2](#) reviews GP modeling. [Section 3](#) begins by extending that review to include historical context for state-of-the-art large scale GPC, ultimately arguing that Vecchia with ESS has the potential to provide high-fidelity, fully Bayesian inference without compromise. [Section 4](#) provides implementation details, illustrations on pedagogical examples, and ultimately application on the BBH simulator. [Section 5](#) introduces deep GP extensions and additional benchmarking. [Section 6](#) concludes with a discussion and directions for future work.

2 Background

Here we provide a foundational description of GP surrogate modeling, first in the context of regression before extending to classification. We also provide a survey of modern GPC methods in order to frame our main contributions beginning in [Section 3](#).

2.1 Gaussian process regression

Consider a black-box simulator $y = f(x)$, where $x \in \mathbb{R}^d$ is the input, and $y \in \mathbb{R}$ is the output. Let $X = [x_1^\top, \dots, x_n^\top]$ be an $n \times d$ matrix collecting n inputs, and let $Y = (y_1, \dots, y_n)^\top$ be a column n -vector of outputs. A GP model assumes $Y \sim \mathcal{N}_n(0, \Sigma(X))$, where $\Sigma(X)$ is an $n \times n$ covariance matrix built using rows of X . The construction of $\Sigma(X)$ depends on our choice of *kernel*, $\Sigma(x_i, x_j) \equiv \Sigma(X)^{ij} \equiv \Sigma(X, X)^{ij}$, which determines the pairwise correlation between outputs y_i and y_j , often in terms of (inverse) distance between their inputs. One common choice is the *squared-exponential* kernel,

$$\Sigma(x, x') = \tau^2 \exp \left\{ -\frac{\|x - x'\|^2}{\theta} \right\}. \quad (1)$$

Our work here is largely agnostic to kernel choice. Many kernels (Abrahamsen, 1997) have forms similar to Eq. (1), where hyperparameters θ and τ^2 determine the distance–correlation strength (lengthscale) and the overall amplitude of the function (scale), respectively.

The MVN form of $Y | X$ elicits a likelihood, say for any hyperparameters in Σ , that is proportional to

$$\mathcal{L}(Y | X) \propto |\Sigma(X)|^{-\frac{1}{2}} \exp \left\{ -\frac{1}{2} Y^\top \Sigma(X)^{-1} Y \right\}. \quad (2)$$

One may maximize (the log of) Eq. (2) with respect to θ and τ^2 to obtain point estimates (Gramacy, 2020). We instead opt for a Bayesian approach that combines information from the likelihood with that from a prior. For τ^2 , an independent inverse-Gamma prior is conjugate, and in fact can be marginalized out analytically (Gramacy, 2020). Unfortunately there is no known conjugate prior choice for θ ; Metropolis-Hastings (MH) can be used to obtain samples from its posterior (Hastings, 1970).

Settings for these hyperparameters are rarely of direct interest; rather their value lies in how they capture input–output dynamics through $\Sigma(X)$ and how that extends to *predictions* for novel inputs $\mathcal{X} \in \mathbb{R}^{n' \times d}$. First consider fixed hyperparameter values, either MLE estimates or a single sample from the posterior. Let $\Sigma(\mathcal{X})$ be defined analogously to $\Sigma(X)$ via pairs in \mathcal{X} , both tacitly conditioned on the same hyperparameters. Similarly populate $\Sigma(\mathcal{X}, X)$, an $n' \times n$ matrix with $(ij)^{th}$ entry defined by the kernel calculation between the i^{th} row of \mathcal{X} and j^{th} row of X . A joint model between observed Y and unknown \mathcal{Y} is $(n + n')$ -variate MVN with mean zero and covariance matrix composed block-wise of $\Sigma(X)$, $\Sigma(\mathcal{X})$, $\Sigma(\mathcal{X}, X)$, and $\Sigma(\mathcal{X}, X)^\top$. Standard MVN conditioning yields

$$\begin{aligned} \mathcal{Y}(\mathcal{X}) | X, Y &\sim \mathcal{N}_{n'}(\mu_{\mathcal{Y}}(\mathcal{X}), \Sigma_{\mathcal{Y}}(\mathcal{X})), \text{ where } \mu_{\mathcal{Y}}(\mathcal{X}) = \Sigma(\mathcal{X}, X)\Sigma(X)^{-1}Y \\ &\Sigma_{\mathcal{Y}}(\mathcal{X}) = \Sigma(\mathcal{X}) - \Sigma(\mathcal{X}, X)\Sigma(X)^{-1}\Sigma(\mathcal{X}, X)^\top. \end{aligned} \quad (3)$$

These are sometimes referred to as the *kriging equations* (Matheron, 1963). In a Bayesian setting, we may filter posterior samples $\{(\theta^{(t)}, \tau^{2(t)})\}_{t=1}^T$ through Eq. (3) to obtain samples for predictive moments $\mu_{\mathcal{Y}}^{(t)}(\mathcal{X})$ and $\Sigma_{\mathcal{Y}}^{(t)}(\mathcal{X})$. These may in turn be used to generate $\mathcal{Y}^{(t)}$ samples via MVN draws, providing a Monte Carlo (MC) approximation to the posterior for \mathcal{Y} . Each batch of hyperparameters requires new calculation of covariance matrices, with subsequent inversion of $\Sigma(X)$ at $\mathcal{O}(n^3)$ computational cost.

2.2 Gaussian process classification

Now suppose outputs are binary, i.e., $y_i \in \{0, 1\}$ for $i = 1, \dots, n$, with some probability $p(x_i)$ of $y_i = 1$, and $1 - p(x_i)$ of $y_i = 0$. Our earlier development for $f(x) : \mathbb{R}^d \rightarrow \mathbb{R}$ is not readily applicable as a model for probabilities $p(x) \in [0, 1]$. But we can follow the generalized linear modeling (GLM; e.g., McCullagh and

Nelder, 1989) approach of deploying an *inverse-link function*, $p(x_i) = \sigma(f(x_i))$ for any monotonic sigmoid $\sigma : \mathbb{R} \rightarrow [0, 1]$. In our work we privilege the canonical logit link, whose inverse is the logistic function $\sigma(z) = \frac{1}{1 + e^{-z}}$; however, our development is not tied to this particular choice. With $y_i \sim \text{Bern}(\sigma(z_i))$, posterior inference for *latent* Z -values may commence through the Bernoulli likelihood

$$\mathcal{L}(Y | Z) = \prod_{i=1}^n \sigma(z_i)^{y_i} (1 - \sigma(z_i))^{1-y_i}. \quad (4)$$

Bayesian formulations hinge on the prior for Z . Albert and Chib (1993) chose linear $Z | X \sim \mathcal{N}_n(X\beta, \mathbb{I}_n\tau^2)$, where data augmentation and Gibbs samplers work well (Frühwirth-Schnatter and Frühwirth, 2010).

With a GP prior, e.g., $Z | X \sim \mathcal{N}_n(0, \Sigma(X))$, Bayesian inference is similar but fraught with challenges because everything involving Z requires cubic-in- n flops. Elliptical slice sampling (Murray et al., 2010) was developed to extend the Gibbs-like posterior sampling framework from Bayesian linear classification to GPs. We shall return to ESS in Section 3.2, for now remarking that fully Bayesian posterior sampling of an n -variate latent Z is considered cumbersome because it exacerbates cubic computational issues.

Early practitioners of GP classification preferred point-inference techniques based on the Laplace approximation (Williams and Barber, 1998) and the like. This approach subsequently became enshrined as canonical for GP classification in machine learning (Rasmussen and Williams, 2006, Chapter 3). Things have evolved somewhat over the last twenty years; the standard benchmark is now a variational approximation (e.g., Damianou et al., 2016) with a low rank, inducing points-based GP covariance (Snelson and Ghahramani, 2006; Titsias, 2009; Banerjee et al., 2013). More recently, a “doubly stochastic” variational inference (DSVI) method has become popular for both ordinary and “deep” GPC modeling (Salimbeni and Deisenroth, 2017). The downside to point-wise inference is reduced UQ, as happens when integration is replaced with maximization. When UQ is essential, such as in active learning for computer experiments, authors have gone to great lengths to avoid *both* point-inference and MCMC (Gramacy and Polson, 2011) while remaining computationally tractable. Approximating the covariance structure helps with computation, but low-rank approximations still blur predictions and sacrifice fidelity (Wu et al., 2022).

2.3 An illustration

In order to illustrate several of these concepts at once, Figure 1 provides a caricature contrasting GP regression (left) with GP logistic classification (right), where the latter uses a latent Z following the same sinusoid as the former. In the classification context the Z -values remain unobserved. Consequently, there can be a great degree of posterior uncertainty in these quantities, both in- and out-of-sample, as indicated by the wider prediction intervals in the right panel compared to the left, both from fully Bayesian fits. The nonparametric nature of the GP prior on Z allows for more flexibility than a linear model, which would struggle to go “back-and-forth” between the alternating regimes without a basis expansion. This makes GP inference conceptually more nuanced than the (Bayesian) linear case, even if operationally they are similar because they involve an MVN prior. For classification, the fully Bayesian GP (blue) gives “crisper” probabilities than the DSVI GP (red). Note that the library we used for DSVI, described later, does not furnish a predictive interval for the latent quantities; i.e., no UQ.

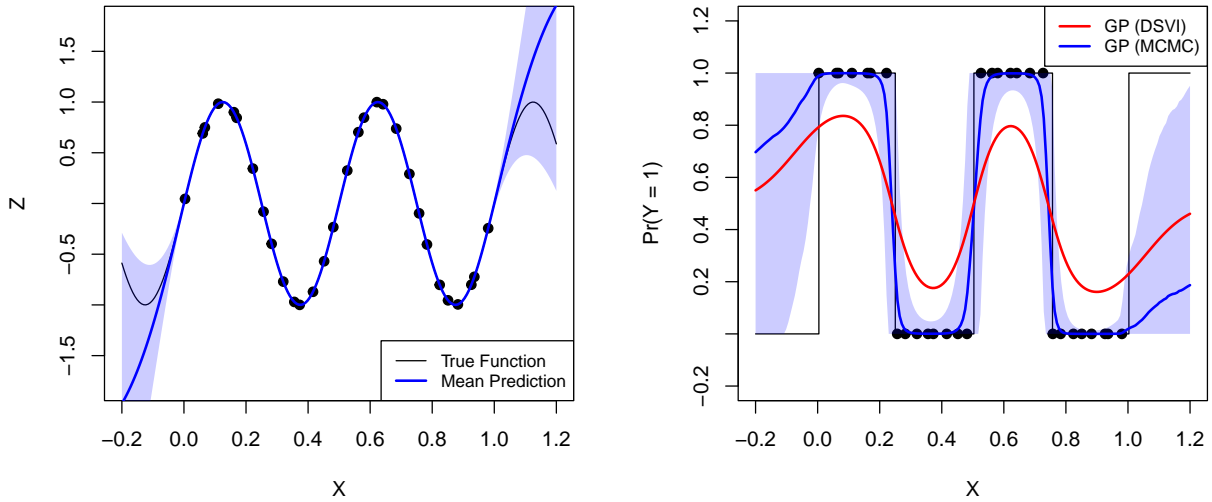


Figure 1: GP predictions from regression and classification models. Real-valued response data Y from a sine function (*left*) is “binarized” into 0’s and 1’s based on the boolean $Y > 0$ (*right*). Fully Bayesian GP(C) shown in blue with 95% prediction interval shaded; DSVI GPC shown in red.

3 Modernizing an old idea for Bayesian GPC

We wish to make predictions for an unknown label y at a novel input x , through probabilities $p_y(x) \equiv \mathbb{P}(y(x) = 1)$, while marginalizing over all *a posteriori* possible latent z -values:

$$\begin{aligned}
 p_y(x) &= \int_{\mathbb{R}} \sigma(z(x)) \cdot p(z(x) | X, Y) dz = \int_{\mathbb{R}} \int_{\mathbb{R}^n} \sigma(z(x)) \cdot p(z(x), Z | X, Y) dZ dz \\
 &= \int_{\mathbb{R}} \int_{\mathbb{R}^n} \sigma(z(x)) \cdot p(z(x) | Z, X, Y) \cdot p(Z | X, Y) dZ dz. \quad (5)
 \end{aligned}$$

The integral above is written to express the simplest case, univariate over a single z at arbitrary x . Our focus is on the inner-integral calculating $p(z(x) | X, Y)$ by marginalizing over the posterior for Z given training data (X, Y) . Conditional on Z , $p(z(x) | Z, X)$ is a straightforward application of GP prediction via Eq. (3), albeit with Z instead of Y , which can be performed separately for each x of interest, or jointly for \mathcal{Y} via \mathcal{Z} over a set of \mathcal{X} ’s. Hyperparameters, such as lengthscales θ , would also require posterior marginalization. We first focus on integrating over $p(Z | X, Y)$ in Sections 3.1–3.3, and then return to prediction and hyperparameter inference in Section 3.4.

Marginalizing over $p(Z | X, Y)$ requires integrating over \mathbb{R}^n , and there is no known closed form. VI/Laplace methods work around this via approximation combined with optimization. We reviewed some of these in Section 2.2 while Rasmussen and Williams (2006, Section 3.3, pp., 41) provide a more complete list. The reason for VI’s popularity is complicated, and has as much to do with circumstance as with technology at the turn of the 21st century. So we indulge in a quick historical digression to help frame our novel contribution in spite of many elements being established over a decade ago.

3.1 Historical digression

The state-of-the-art in fully Bayesian GPC at the end of the 20th century involved Metropolis samplers (Neal, 1998). Although tuning and blocking helped, these generally produced sticky chains and slow convergence in n -dimensional latent Z space and were only practical for $n < 100$ or so. Laplace methods (Williams and Barber, 1998) and those based on expectation propagation (Minka, 2001), a variant of VI, broke through that barrier in a big way. About a decade later Murray et al. (2010) solved the MCMC/Metropolis mixing problem for latent GPs, of which GPC was one example. Despite the simplicity of their ESS algorithm [Section 3.2] it didn’t catch on. MCMC via ESS was slower than Laplace/VI, and as problems got bigger ($n \gg 1,000$) cubic-in- n complexity meant that thousands of MCMC iterations – even with excellent mixing – couldn’t compete with mere dozens of Newton-like iterations. It was better to get something in a reasonable amount of time than to get nothing after waiting forever.

As problems became even bigger ($n \gg 10,000$) many practitioners leveraged sparse or low-rank approximations to Σ (e.g., Melkumyan and Ramos, 2009; Emery, 2009; Gramacy and Apley, 2015; Cole et al., 2021; Quinonero-Candela and Rasmussen, 2005; Lázaro-Gredilla et al., 2010) to avoid cubic bottlenecks. One particular low-rank approximation, now known as inducing points, turned out to be particularly well-suited for VI. But IP approximations offer low-resolution in large n settings; where a wealth of data ought to reveal a rich and nuanced response surface, GPC via VI/IP instead oversmooths, like in Figure 1.

Recently, there has been renewed interest in the Vecchia (1988) approximation for GP regression as an alternative to IPs (e.g., Katzfuss et al., 2020; Datta, 2021; Stein et al., 2004; Stroud et al., 2017; Datta et al., 2016; Katzfuss and Guinness, 2021; Katzfuss et al., 2022). It turns out, as we will show shortly in Section 3.3, Vecchia is ideally suited to (by now long forgotten) ESS for GPC. We are not the first to apply Vecchia in the context of GPC, or other latent Gaussian models (e.g., Zilber and Katzfuss, 2021; Cao et al., 2023), but we are the first to do so in a fully Bayesian context via ESS.

3.2 Elliptical slice sampling

The hard part of Eq. (5) is integrating $p(Z | X, Y)$ over $Z \in \mathbb{R}^n$, which is high dimensional and analytically intractable. Bayes rule provides $p(Z | X, Y) \propto p(Y | Z) \cdot p(Z | X)$ where $p(Y | Z)$ is the Bernoulli likelihood from Eq. (4), and $p(Z | X)$ is the GP prior $Z \sim \mathcal{N}_n(0, \Sigma(X))$, which is not conjugate for that likelihood. Murray et al.’s elliptical slice sampling algorithm is designed exactly for this setting: MVN prior with arbitrary likelihood. ESS is inspired by (ordinary) slice sampling (SS; Neal, 2003) which is more general in one sense (any prior/target distribution) but more specific in another (one-dimensional sampling).

Algorithm 1 provides the details. It is worth clarifying that any log likelihood $\ell(\cdot)$ may be used, with any MVN prior $\mathcal{N}(\mu, \Sigma)$. ESS is not particular to GPC; Murray et al. (2010) included GPC as an example among others. Like SS, ESS is a “rejection-free” method in that only a single random proposal $Z' \sim \mathcal{N}_n(0, \Sigma(X))$ is required, and a quantity calculated from Z' , and possibly other random scalars, is eventually returned. It establishes a Markov chain because the returned quantity $Z^{(t+1)}$ is a function of both Z' and the previous sample $Z^{(t)}$. In contrast to Metropolis samplers, $Z^{(t+1)}$ is never a copy of the previous sample ($Z^{(t+1)} \neq Z^{(t)}$). Like rejection sampling (Robert et al., 1999), ESS has a loop over random deviates, but unlike rejection sampling each iteration increases the probability of ultimate acceptance.

To illustrate ESS for GPC, consider the “top-hat” example (Dunlop et al., 2018) shown in the top-left panel of Figure 2. The response steps from $y(x_i) = 0$ to 1 and back again as x_i varies from left to right. We observe Y values at a Latin hypercube sample (LHS; McKay et al., 1979) X of size $n = 50$. Our GP prior assumes $Z \sim \mathcal{N}(0, \Sigma(X))$, where $\Sigma(X)$ follows the squared-exponential kernel (1) with fixed $\theta = 0.1$. We obtain $T = 5,000$ posterior samples from $Z | X, Y$ following Alg. 1 for $t = 1, \dots, T$, beginning with $z_i^{(1)} = \log(-2\tau)$ if $y_i = 0$, and $z_i^{(1)} = \log(2\tau)$ if $y_i = 1$, where τ is chosen via a heuristic discussed

Algorithm 1: Elliptical slice sampling for GPC estimation.

Input: Previous $Z^{(t)}$, response Y , covariance $\Sigma(X)$, log likelihood ℓ .

Output: Posterior sample $Z^{(t+1)} \sim p(Z|X, Y)$.

Draw $Z' \sim \mathcal{N}_n(0, \Sigma(X))$.

Draw $u \sim \text{Unif}[0, 1]$ and set acceptance threshold $\ell_{\text{thresh}} = \ell(Y | Z^{(t)}) + \log(u)$.

Draw angle $\gamma \sim \text{Unif}[0, 2\pi]$. Construct bracket $\gamma_{\min} = \gamma - 2\pi$, $\gamma_{\max} = \gamma$.

while 1 **do**

 Calculate proposal $Z^* = Z^{(t)} \cos(\gamma) + Z' \sin(\gamma)$ and evaluate $\ell_{\text{prop}} = \ell(Y | Z^*)$.

if $\ell_{\text{prop}} > \ell_{\text{thresh}}$ **then**

 Return $Z^{(t+1)} = Z^*$.

else

if $\gamma < 0$ **then**

 Return $\gamma_{\min} = \gamma$

else

 Return $\gamma_{\max} = \gamma$

 Draw new $\gamma \sim \text{Unif}[\gamma_{\min}, \gamma_{\max}]$.

later in Section 4.1. This took about five seconds on a conventional, single-core workstation, or about one thousandth of a second per draw. Each ESS sample required around six loop iterations on average, but sometimes as few as one or as many as fourteen. The remaining samples after a burn-in of 1,000 and a thinning rate of 10 are shown as gray lines in the top-right panel of the figure. Notice each $Z^{(t)}$ is a smooth, continuous realization. The bottom-left panel shows raw chains, samples $z_i^{(1)}, \dots, z_i^{(T)}$, for three indices $i \in \{1, 25, 35\}$. These showcase the GPC’s varying confidence in a 1-label depending on an input’s closeness to transitions between classes. Lastly, the bottom-right panel provides the median and 95% interval for the autocorrelation of our samples across all $n = 50$ training observations. These showcase the sampler’s excellent mixing and ability to avoid getting “stuck,” as a Metropolis sampler might.

Besides its simplicity, perhaps the most important takeaway from Alg. 1 – which we repeat here for emphasis – is that only one MVN instance Z' is required for each $Z^{(t)} \rightarrow Z^{(t+1)}$. Besides evaluating log likelihoods, which for our Bernoulli GPC setup requires flops linear in n , the only real work lies in generating $Z' \sim \mathcal{N}_n(0, \Sigma(X))$. If you were looking to make ESS for GPC more computationally efficient, say, to handle larger n in a reasonable amount of time, this is where you would target your effort. In Section 4.3 we explore the BBH example with n in the tens of thousands, which is not tractable for even one MCMC iteration, let alone hundreds or thousands, no matter how good ESS mixing is.

Although there are many algorithms for MVN sampling, the most common is via Cholesky decomposition. Gelman et al. (1995) explain that one may convert n independent standard normal deviates $\xi = (\xi_1, \dots, \xi_n)$ into MVN ones via $Z' = \mu + U\xi$, where U is a Cholesky factor for Σ , or $\Sigma(X) = UU^\top$. Calculating U is cubic in n for dense matrices Σ . The Vecchia approximation (Vecchia, 1988), discussed next, may be the most expedient way of generating a sparse Cholesky factor for covariance matrices $\Sigma(X)$ based on inverse distance. Although Vecchia-based GP approximation has seen a resurgence of interest lately for GP likelihoods (2) and predictive equations (3), as we have already reviewed, we are the first to recognize its value in the context of GPC via ESS, where all that’s required are MVN proposals.

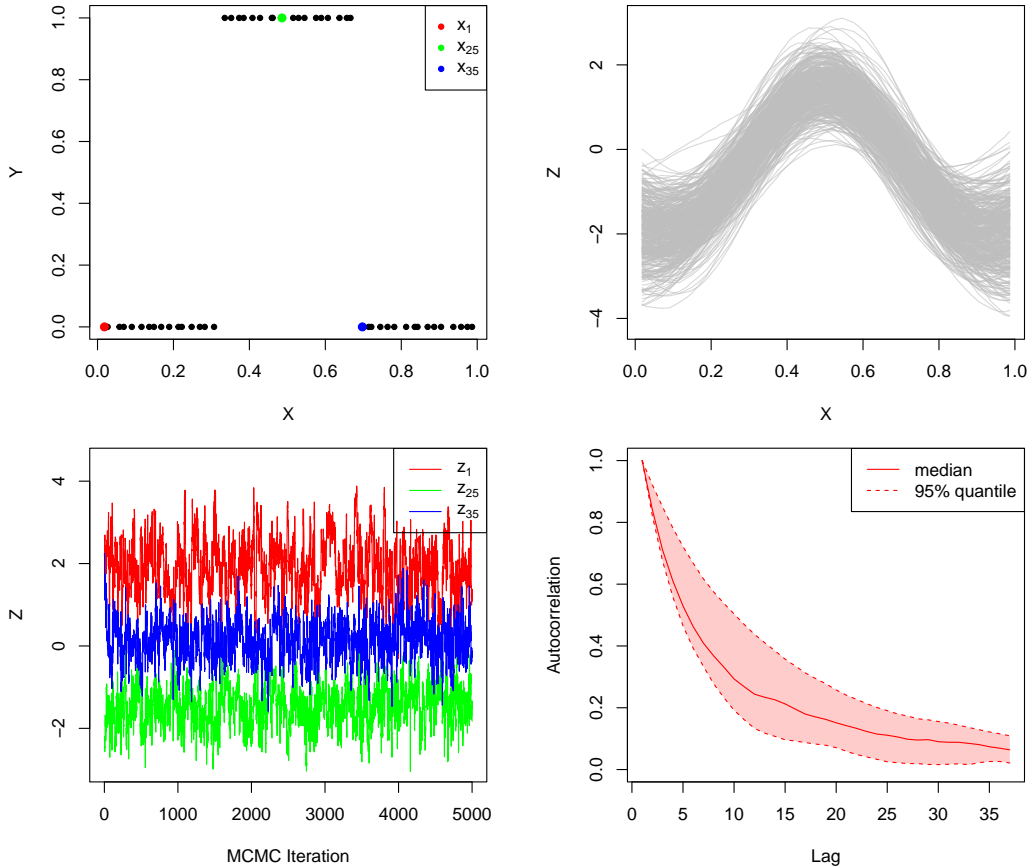


Figure 2: ESS GPC illustration. *Top-left*: training data with “top-hat” response. *Top-right*: samples of $Z^{(1:T)}$ after burn-in and thinning. *Bottom-left*: chain of $z^{(t)}$ values at x_1 , x_{25} and x_{35} . *Bottom-right*: autocorrelation distribution (median and 95% quantiles) for all $Z^{(1:T)}$.

3.3 Vecchia approximation

At its core, [Vecchia \(1988\)](#)’s idea for approximating MVN likelihoods is simple. Any joint probability distribution may be formulated as a product of cascading conditionals $p(z_1, z_2, z_3) = p(z_3 | z_2, z_1)p(z_2 | z_1)p(z_1)$, in any order or indexing. An approximation may be obtained by dropping some of the conditioning variables, e.g., $p(z_1, z_2, z_3) \approx p(z_3 | z_1)p(z_2 | z_1)p(z_1)$. This is applicable to any distribution, but the quality of the approximation depends on many factors. In the case of MVNs, two remarks are noteworthy: (i) those conditional distributions are (univariate) Gaussian and have a convenient closed form [\(3\)](#); (ii) the computations within this closed form will involve smaller matrices if conditioning variables are reduced.

Although that description is intuitive, modern Vecchia for GPs is not done through products of conditional distributions. Rather, computations leverage the fact that dropping conditioning variables induces conditional independence. In other words, $p(z_3 | z_1)p(z_2 | z_1)p(z_1)$ encodes that z_3 is independent of z_2 given z_1 . Conditional independence equates to zeros in the inverse covariance (a.k.a., precision) matrix. A modern Vecchia approximation induces sparsity in the MVN precision matrix for an n -dimensional Z .

Most recent literature on Vecchia (e.g., [Katzfuss et al., 2020](#); [Datta et al., 2016](#)) focuses on aspects of the approximation that target the regression GP setting, including its effect on the the full, joint likelihood [\(2\)](#), and other aspects of Bayesian inference including predictive equations [\(3\)](#). These details do not pertain

directly to the classification context, at least when ESS is used, although they shall be relevant later when we discuss broader aspects of our sampling procedure in Section 3.4 and our deep GP enhancements in Section 5. As we explain in Section 3.2, the most expensive operation in ESS sampling for GPC is generating MVN proposals. Here we leverage a result from [Katzfuss and Guinness \(2021\)](#), which shows how the precision matrix can be written as an upper–lower Cholesky decomposition: $\Sigma(X)^{-1} = UU^\top$.

Let $c(i) \subseteq \{1, \dots, i-1\}$ denote the conditioning set for the i^{th} variate in the MVN for $i = 1, \dots, n$, i.e., describing the univariate conditional $z_i \mid Z_{c(i)}$. Also let $X_{c(i)}$ denote the rows of X corresponding to $Z_{c(i)}$ for a GP. [Katzfuss and Guinness](#) show how entries of the $n \times n$ triangular matrix U can be calculated as

$$U_X^{ji} = \begin{cases} 1 & i = j \\ \frac{1}{\sigma_i(X_{c(i)})} & j \in c(i) \\ -\frac{1}{\sigma_i(X_{c(i)})} \Sigma(x_i, X_{c(i)}) \Sigma(X_{c(i)})^{-1} [\text{index of } j \in c(i)] & j \in c(i) \\ 0 & \text{otherwise,} \end{cases} \quad (6)$$

where $\sigma_i^2(X) \equiv \Sigma_Z(x_i) = \Sigma(x_i) - \Sigma(x_i, X) \Sigma(X)^{-1} \Sigma(X, x_i)$, i.e., following Eq. (3) with singleton $\{x\} = \mathcal{X}$. Several details are worth noting here. First, U^{ji} entries may be populated in parallel as they only depend on X , conditioning indices $c(i)$, and covariance hyperparameters. In our implementation (more details in Section 4.1) we populate this matrix via `OpenMP` for symmetric multi-core speedups. If we limit the conditioning set size to a maximum of m variables ($|c(i)| \leq m$), then each U^j row can be calculated in time $\mathcal{O}(m^3)$, owing primarily to the cost of decomposing the $(m \times m)$ -dimensional matrix $\Sigma(X_{c(i)})$. Populating all n rows of U requires flops in $\mathcal{O}(nm^3)$, which is a substantial improvement over the usual $\mathcal{O}(n^3)$ cost of a Cholesky decomposition when $m \ll n$.

For our purposes (ESS for GPC), this means the following: proposals $Z' \sim \mathcal{N}_n(0, \Sigma(X))$ may be drawn by first sampling $a_1, \dots, a_n \stackrel{\text{iid}}{\sim} \mathcal{N}(0, 1)$, then calculating $Z' = (U^\top)^{-1}a$. A simple rearrangement yields the form $U^T Z' = a$, where Z' can be found via a sparse forward solve and, crucially, without the need to directly invert U ([Sauer et al., 2022a](#)). In subsequent ESS iterations, if hyperparameters are fixed – or if they are otherwise identical to those used in the previous draw because a Metropolis proposal for the lengthscale was rejected – one may proceed without re-calculating U . The quality of the approximation depends on the conditioning set size, m , and the selection of $c(i)$. We follow [Sauer et al.](#) in choosing $m = 25$ and additional specifications provided along with other implementation details in Section 4.

To showcase the speed-up Vecchia provides to GPC training, consider the simulated 2d “box” example ([Broderick and Gramacy, 2011](#)) shown in the left panel of Figure 3. The middle panel compares the run-time for training a GPC to data from this surface using $T = 5,000$ MCMC iterations, with and without Vecchia. For both, we fix $\theta = 1$ (later estimated in Section 3.4) and $\tau^2 = 25$ (discussed in more detail in Section 4.1) to focus our comparison on the time required for latent Z sampling. Observe that as the training size n increases, the “full” GPC takes drastically longer, while the Vecchia version only sees a slight bump in run-time. The right panel compares predictive accuracy from 10 different LHS design constructions on a separate LHS testing set of size $n' = 500$. Details are in Section 3.4; the main takeaway here is that the Vecchia-approximated GPC performs similarly to the full one.

3.4 Full posterior sampling and prediction

Here we complete the description of our Bayesian inferential framework for all unknown quantities, connecting Sections 3.2–3.3 with the ultimate goal of furnishing predictions (5). Algorithm 2 outlines the ESS/Metropolis-within-Gibbs procedure we use for MC integration over latent Z and lengthscale θ . Recall, θ is tacitly involved in $\Sigma(X)$, and therefore also in U via Eq. (6).

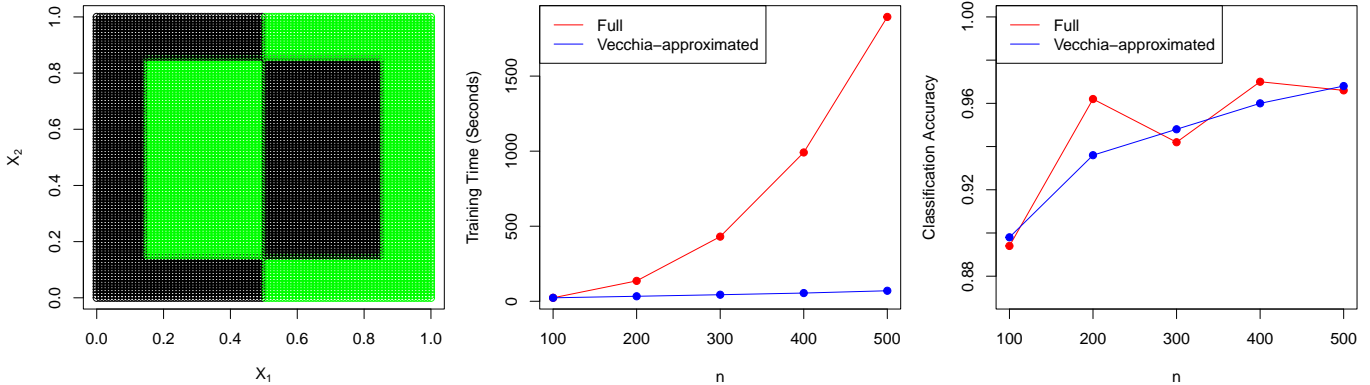


Figure 3: *Left*: 2d “box” example. *Middle*: run-times for “full” and Vecchia-approximated ($m = 25$) GPC training. *Right*: classification accuracy from various GPCs.

Algorithm 2: Gibbs sampling procedure for GPC estimation.

```

Initialize  $\theta^{(1)}, Z^{(1)}$ 
for  $t = 2, \dots, T$  do
     $\theta^{(t)} \sim \pi(\theta | X, Z^{(t-1)})$  // MH via  $\mathcal{L}(Z | X, \theta)$ 
     $Z^{(t)} \sim \pi(Z | X, Y, \theta^{(t)})$  // ESS via  $\mathcal{L}(Z | X, \theta), \mathcal{L}(Y | Z)$ 

```

Posterior sampling of Z involves Vecchia-approximated MVN proposals within ESS (Alg. 1), where acceptance is based on the Bernoulli likelihood (4). Posterior sampling of θ employs Metropolis Hastings, where acceptance probabilities utilize the MVN likelihood of Eq. (2), again with Z in place of Y . This calculation requires an $n \times n$ inverse and determinant. Usually these are furnished by a single Cholesky decomposition, which means the Vecchia approximation is again handy here. In fact, speedy MVN likelihood calculations are the most common application of Vecchia in the literature (e.g., [Katzfuss et al., 2020](#); [Datta et al., 2016](#)). The details are provided here for completeness:

$$\begin{aligned}
 \mathcal{L}(Z | X) &\propto |\Sigma(X)|^{-\frac{1}{2}} \exp \left\{ -\frac{1}{2} Z^\top \Sigma(X)^{-1} Z \right\} \\
 &\approx \sum_{i=1}^n U^{ii} \cdot \exp \left\{ -\frac{1}{2} Z^\top U U^\top Z \right\}.
 \end{aligned}$$

Given X and $\theta^{(t)}$, U might be more aptly notated as $U^{(t)}(X)$, but we opt to keep it simple. Since U uses $\theta^{(t)}$, it must be reconstructed if a new θ -value is accepted. As with MVN proposals in Section 3.3, the computational order for likelihood evaluation under Vecchia is $\mathcal{O}(nm^3)$. Additional details on our prior and proposal mechanism for θ , along with choices of initial values $(\theta^{(1)}, Z^{(1)})$, are reserved for Section 4.1.

We pivot now to prediction. Suppose we have a collection of testing inputs $\mathcal{X} \in \mathbb{R}^{n' \times d}$ where we wish to assess $\mathcal{Y}(\mathcal{X}) | X, Y$. In the context of a single predictive location $x \in \mathcal{X}$, Eq. (5) explains that after we integrate over Z [Section 3.3 and Alg. 2], all that remains is to generate $z(x) | Z, X$ and apply the sigmoid $\sigma(z(x))$. Here we flesh out the details of prediction vectorized over all $\mathcal{Z} \equiv \mathcal{Z}(\mathcal{X})$. Given a sample of $Z^{(t)}$ -values, we may draw $\mathcal{Z}^{(t)}$ -values via Eq. (3), again with $Z^{(t)}$ and $\mathcal{Z}^{(t)}$ rather than Y and \mathcal{Y} , which may be computationally fraught without approximation. As a workaround, we appropriate [Sauer et al.](#)

(2022a)’s simplified Vecchia scheme, which may be described as follows.

First form $X^{\text{stack}} = [X; \mathcal{X}]$ by stacking one after the other, row-wise, letting $i = 1, \dots, n, n+1, \dots, n+n'$ index the rows. Note, testing locations must be indexed *after* training ones. Next extend conditioning sets $c(i)$ for $i = n+1, \dots, n+n'$ to include any indices $j < i$, meaning testing locations might condition on other testing locations. Then, apply Eq. (6) with the combined X^{stack} in place of X to obtain what we refer to as U^{stack} . This matrix is still sparse and upper triangular, with at most m -many non-zero off-diagonal elements in each column. We may partition U^{stack} as follows,

$$U^{\text{stack}} = \begin{bmatrix} U_X & U_{X,\mathcal{X}} \\ 0 & U_{\mathcal{X}} \end{bmatrix},$$

where U_X is the original upper triangular matrix formed from Eq. (6) with X alone. Then, one may derive the following predictive equations:

$$\mathcal{Z}^{(t)} \mid X, Y, Z^{(t)}, \theta^{(t)} \sim \mathcal{N}_{n'}(\mu^*, \Sigma^*) \quad \text{where} \quad \mu^* = -(U_{\mathcal{X}}^\top)^{-1} U_{X,\mathcal{X}}^\top Z^{(t)} \quad \text{and} \quad \Sigma^* = \left(U_{\mathcal{X}} U_{\mathcal{X}}^\top \right)^{-1}. \quad (7)$$

Again, note both μ^* and Σ^* tacitly depend on $\theta^{(t)}$ via $U_{\mathcal{X}}$ and $U_{X,\mathcal{X}}$. Sampling from this MVN can be computationally intensive for $d > 1$, even with Vecchia applied. One way to further speed up prediction is to draw predictive samples at individual entries in \mathcal{X} via their univariate normals. While pointwise prediction neglects covariances across out-of-sample observations, we have found predictions are nonetheless very similar. We therefore utilize this shortcut in all of our experiments moving forward.

Samples $\mathcal{Z}^{(t)}$ collected over $t = 1, \dots, T$ may be converted into assessments of $p_y(\mathcal{X})$, completing our vectorized approximation to Eq. (5), through the laws of total expectation and variance:

$$\begin{aligned} \hat{\mu}_y(\mathcal{X}) &= \frac{1}{T} \sum_{t=1}^T \sigma \left(\mathcal{Z}^{(t)} \right) \\ \hat{\sigma}_y^2(\mathcal{X}) &= \frac{1}{T-1} \sum_{t=1}^T \left(\sigma \left(\mathcal{Z}^{(t)} \right) - \hat{\mu}_y(\mathcal{X}) \right)^\top \left(\sigma \left(\mathcal{Z}^{(t)} \right) - \hat{\mu}_y(\mathcal{X}) \right) + \frac{1}{T} \sum_{t=1}^T \sigma \left(\mathcal{Z}^{(t)} \right) \left(1 - \sigma \left(\mathcal{Z}^{(t)} \right) \right). \end{aligned} \quad (8)$$

The first term in Eq. (8) for $\hat{\sigma}_y^2(\mathcal{X})$ represents uncertainty in the model’s estimated probability of success, while the second stems from inherent variability contained in the random Bernoulli draw which produced the binary output. The latter component increases as estimated probabilities approach 0.5, where drawing $y(x)$ becomes essentially a coin flip. A classification rule can be formed from any threshold on $\hat{\mu}_y$; however, in our own work (such as the right panel of Figure 3), we stick with the 50:50 rule: $\hat{y}(x_i) = \mathbb{1}(\hat{\mu}_y(x_i) \geq 0.5)$.

To continue the illustration, consider Figure 4, which provides views of $\hat{\mu}_y(\mathcal{X})$ and $\hat{\sigma}_y^2(\mathcal{X})$ from Eq. (8) in its left and right panels, respectively. As in Figure 3 we use $m = 25$, but for this illustration we fix $n = 200$ via LHS and use a regular predictive grid for \mathcal{X} with a total of $n' = 10,000$ rows. Notice the mean predictions in the left panel capture the general form of the box shape in the response surface. The uncertainty shown in the right panel highlights boundary regions dividing class labels. This makes intuitive sense; uncertainty is highest in locations where the response transitions from success to failure.

4 Implementation and empirical results

Here we provide implementation details for our proposed GPC model, and assess its performance in both simulated examples and the motivating binary black hole example introduced in Section 1.

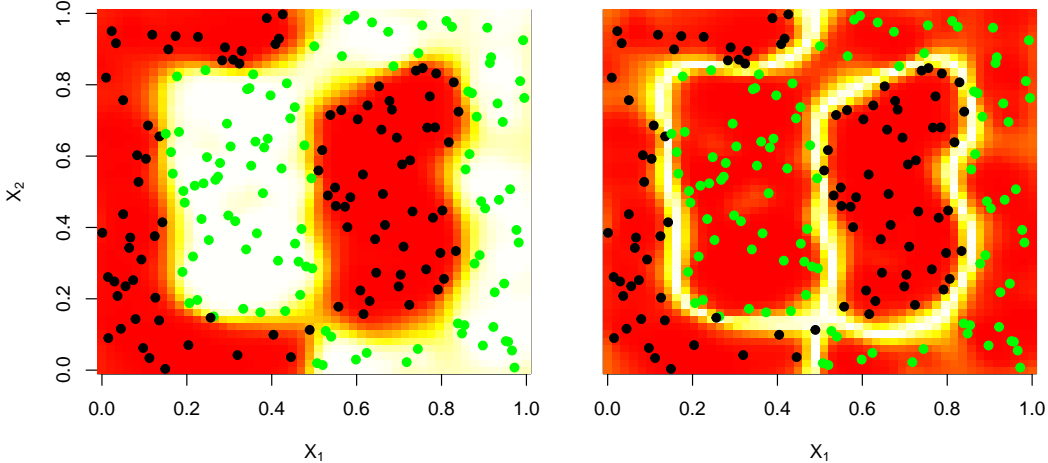


Figure 4: Posterior mean (*left*) and variance (*right*) of $p_y(\mathcal{X})$ for the 2d “box” example [Figure 3] produced by a Vecchia-approximated GPC. Brighter colors indicate larger values.

4.1 Implementation details

Our implementation allows for either the squared-exponential (1) or Matérn $\nu = 5/2$ kernels for $\Sigma(X)$, with the latter performing slightly better in our comparisons. Both require specification of lengthscale θ and scale τ^2 . We fix τ^2 following a simple rule (discussed momentarily) and sample θ via MCMC alternating with Z in a Gibbs-like fashion [Alg. 2]. For all empirical work we take $\theta \sim \text{Gamma}(1.5, 2.6)$ providing a prior spread appropriate for inputs coded, marginally, to the unit interval. Metropolis proposals follow $\theta^{(t)} \sim \text{Unif}\left[u\theta^{(t-1)}, \frac{1}{u}\theta^{(t-1)}\right]$. Throughout we use $u = 2/3$, i.e., proposing $\approx 33\%$ above or below the previous value, since that consistently yields a reasonable acceptance rate. Chains are initialized with $\theta^{(1)} = 0.1$ and $z_i^{(1)} = 2\tau$ or -2τ depending on if $y_i = 1$ or 0, respectively. All chains are run for 10,000 iterations, discarding the first 1,000 as burn-in and thinning by a factor of 10 for a total of $T = 900$.

Although this choice of $Z^{(1)}$ gives decent initial probabilities $\sigma(Z)$ associated with Y , it is not a smooth (or stationary) function of inputs X , and therefore presents a poor initialization of a latent GP. When n is small, burn-in to a smooth GP realization is quick, but for larger n we find it is helpful to introduce a nugget (Gramacy and Lee, 2012) hyperparameter into Σ which captures deviations from a smooth/stationary process as noise (Binois et al., 2018). We only do this for the burn-in portion of our sampling, taking a zero nugget (i.e., no nugget and no noise) afterwards for posterior sampling. During burn-in, we additionally find it helpful to utilize a prior on the nugget that concentrates on zero as sampling iteration t progresses, i.e., $\text{Gamma}(1, 10t)$. The effect of a (non-zero) nugget parameter has long remained one of speculation in the GPC literature, going back to Neal (1998). Our consideration here is somewhat different, focusing on the nugget’s effect on what we would otherwise prefer to be smooth latent quantities, considering our deterministic surrogate modeling context. Binois et al. remark that in their setting, which is similar to but not identical to ours, the maximum *a posteriori* nugget is zero, so there is little harm in concentrating it out artificially, as we do during burn-in via the prior.

Our Vecchia implementation leverages a parallelized construction of U_X , $U_{\mathcal{X}}$ and $U_{X,\mathcal{X}}$, independently distributing rows over multiple cores via `OpenMP` and `RcppArmadillo` (Eddelbuettel and Sanderson, 2014) and as described by Sauer et al. (2022a). Sparse matrix storage and manipulation is furnished via the `Matrix` library (Bates et al., 2010). We use random indexing and nearest neighbors for $c(i)$ as is common

in the literature (e.g., [Stein et al., 2004](#); [Datta et al., 2016](#); [Katzfuss et al., 2020](#)).

We compare the predictive performance of our full (where possible) and Vecchia-approximated GPC predictions to the following benchmark comparators:

- Doubly-Stochastic Variational Inference (DSVI, [Salimbeni and Deisenroth, 2017](#)), implemented in the Python library `GPFlux` ([Dutordoir et al., 2021](#))
- Scalable Variational Gaussian Process (SVGP, [Hensman et al., 2015](#)), implemented in the Python library `GPflow` ([Matthews et al., 2017](#)).

In each of ten repeated MC instances, we randomly generate a training and testing partition of sizes n and n' , respectively, fit the models on the training data, and then use them to predict out-of-sample on the testing set. Throughout, we fix $n' = 1,000$ while varying n over a range that is test-problem dependent. The comparisons coming shortly additionally show a deep (“DGPC”) competitor which can be ignored for now and will be discussed, along with additional analysis and commentary, in [Section 5](#).

Performance metrics include correct classification rate (CR, higher is better) and logarithmic score (LS, higher is better; [Gneiting and Raftery, 2007](#), Table 1). Let y_i denote the true class label associated with testing input $x_i \in \mathcal{X}$, $i = 1, \dots, n'$, collected as \mathcal{Y} . Then, let $\hat{y}_i \equiv \hat{y}(x_i) \mid X, Y$ denote a predicted label given n training examples (X, Y) , collected as $\hat{\mathcal{Y}}$. Similarly let $\hat{p}_i \equiv p_y(x_i) \equiv \mathbb{P}(Y(x_i) = 1 \mid X, Y)$ denote the predicted probability $y_i \in \mathcal{Y}$ is 1, and collect these as $\hat{\mathcal{P}}$. Then CR and LS are defined as follows:

$$\text{CR}(\mathcal{Y}, \hat{\mathcal{Y}}) = \frac{1}{n'} \sum_{i=1}^{n'} \mathbb{1}(y_i = \hat{y}_i) \quad \text{LS}(\mathcal{Y}, \hat{\mathcal{P}}) = -\frac{1}{n'} \sum_{i=1}^{n'} [y_i \log(\hat{p}_i) + (1 - y_i) \log(1 - \hat{p}_i)]. \quad (9)$$

When evaluating our Python comparators on these metrics, we simply take $\hat{\mathcal{P}}$ from the software output directly. For our own methods, we use posterior sampling as described earlier and take $\hat{\mathcal{P}} = \hat{\mu}_y(\mathcal{X})$ following [Eq. \(8\)](#). For all methods we convert $\hat{\mathcal{P}}$ to $\hat{\mathcal{Y}}$ using a threshold of $\hat{\mu}_y(\mathcal{X}) \geq 0.5$.

Choosing an appropriate scale for the reference process

An inverse-gamma (IG) prior on τ^2 is semi-conjugate, meaning conditional posterior inference may be facilitated by analytic integration without MCMC sampling. An (improper) “reference” prior $p(\tau^2) \propto \frac{1}{\tau^2}$, which is mathematically $\text{IG}(0, 0)$, is similarly analytic and thus a common choice in regression GP settings ([Gramacy, 2020](#), Chapter 5). However, we have found that, in our classification setting, posterior integration over τ^2 does not work well because the responses (which are just 0s and 1s) do not provide a strong sense of “scale” for the latent Z process via the Bernoulli likelihood. A practical consequence of this is that posterior draws for τ^2 can be wildly large under a reference prior, translating to very large/small probabilities $\sigma(Z)$ under the logit transform, and likewise ones that are too close to $\sigma(Z) = 0.5$ under stronger priors even when prediction ought to be more confident.

τ^2	2^0	2^1	2^2	2^3	2^4
$\sigma(2^\tau)$	0.881	0.944	0.982	0.997	1.000
$\sigma(-2^\tau)$	0.119	0.056	0.018	0.003	0.000

Table 1: Impact of the choice of τ^2 on tail classification probabilities.

To provide more detail, and ultimately aid in prescribing an appropriate, data-dependent setting for the latent scale, consider the values provided in [Table 1](#). As τ^2 grows from $\tau^2 = 1$ to 16 the table

shows the range of low and high probabilities that could, *a priori*, be realized from Z -values out at 95% interval boundaries. For example, when $\tau^2 = 2^0 = 1$ most Z s are (*a priori*) within $[-2, 2]$ which means $p \in [0.119, 0.881]$ with probability 0.95. Such a range may be appropriate with a small training data set, like $n \leq 10$. Suppose you believed *a priori* that you *could* observe at least one observation in each class, anywhere in the input space. When $n = 10$ that means $p(x) \in [0.1, 0.9]$, i.e., a similar range as in the table for $\tau^2 = 1$. Such a prior could be said to follow a unit-information principle (Jin and Yin, 2021). Now imagine a balanced training data set of $n = 2,000$ points (1000 in each class) were labels are geographically separated from one another. In that case $p(x) = 999/1,000$ or $1/1,000$ is reasonable for any particular x regardless of its location in the input space. A prior for Z via $\tau^2 = 1$ would be a poor match, shrinking $p(x)$ towards $[0.119, 0.881]$ leading to under-confidence and lower scores (9) out-of-sample. Looking at Table 1, a better match to that scenario would be $\tau^2 = 2^3$ so that $p \in [0.003, 0.997]$.

We wish to operationalize this idea into a scheme that provides an automatic determination for τ^2 in a data-dependent way, but crucially avoids “double-dipping” from a Bayesian statistical perspective. To this end, we introduce a concept of a training data point’s degree of *insulation*: $\omega_i \equiv \omega(x_i, y_i)$, which is the size of the (nearest) neighborhood of x_i in the training data set X such that all of x_i ’s neighbors in X agree in label with y_i . Insulation is thereby measuring a degree of local homogeneity. Specifically, let $D = \{d_{ij}\}_{i,j=1}^n$ denote the $n \times n$ pairwise Euclidean distance matrix of X , and define

$$\omega_i = \left| \left\{ x_j \in X^{(-i)} : d_{ij} < \min_{k \neq i} \{d_{ik} : y_k \neq y_i\} \right\} \right|. \quad (10)$$

Now let $\omega^{\max} = \max_{i=1, \dots, n} \omega_i$ denote the degree of the most insulated training data point. The unit-information-prior idea above suggests that a sensible setting for τ^2 could be derived by anchoring to $\omega^{\max}/(\omega^{\max} + 1)$ and its complement $1/(\omega^{\max} + 1)$. Here we introduce a tuning parameter ϵ to entertain an ϵ -information prior via $p_\epsilon^{\max} = \omega^{\max}/(\omega^{\max} + \epsilon)$. Then, invert p_ϵ^{\max} with $\sigma(\cdot)$ to determine the latent z -value; under a logit transform, that is $z_\epsilon^{\max} = \log(p_\epsilon^{\max}/(1 - p_\epsilon^{\max}))$. Finally, determine τ^2 so that z_ϵ^{\max} is two standard deviations from the mean ($z_\epsilon^{\max} = 2\tau$) and solve: $\tau_\epsilon^2 = (z_\epsilon^{\max}/2)^2$.

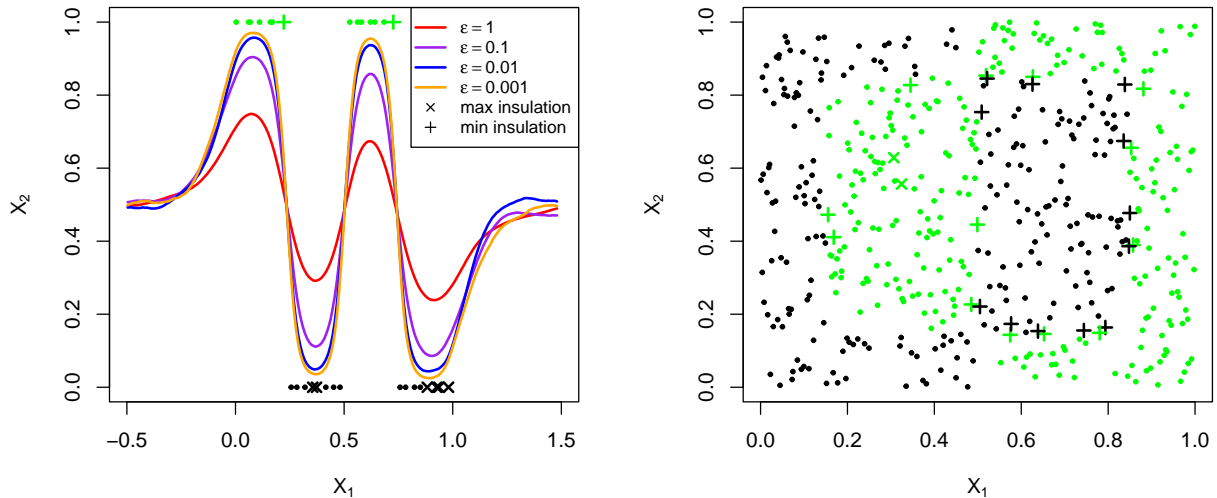


Figure 5: *Left*: Posterior mean $\mu(x)$ for various ϵ values specifying τ^2 on the 1d sin example [Figure 1]. \times ’s denote observations with maximum insulation ($\omega^{\max} = 7$). *Right*: 500 randomly sampled points from the 2d box example [Figure 3], with $\omega^{\max} = 55$. For reference, $+$ ’s indicate minimum insulation.

Two examples are provided in Figure 5, via our earlier 1d [Section 2.3/Figure 1] and 2d [Section 3.4/Figure 4] illustrations. The most-insulated points are indicated with \times 's, where ω^{\max} is 7 for the first example and 55 for the second. A choice of ϵ determines p_ϵ^{\max} and that, in turn, affects the posterior mean prediction from our GPC model, as indicated in the left panel for the 1d example. A unit-information prior ($\epsilon = 1$) would be sensible in many modeling contexts; however, that is a poor choice for this example, and would lead to a washed-out predictive surface (in red). One thing that is special in our context of surrogate modeling for computer simulation experiments is that the data-generating mechanism is deterministic. Thus, for well-insulated data points, the probabilities won't change quickly as we move away from such locations. In other words, we can get away with a much smaller ϵ .

One option is to dial in $\hat{\epsilon}$ via cross-validation (CV). Although this could require substantial work, recognizing additional structure offers some simplification. Observe there is a monotonic relationship between τ_ϵ^2 and p_ϵ^{\max} . As $\epsilon \rightarrow 0$, say beginning from the unit information prior $\epsilon = 1$, we get larger τ_ϵ^2 yielding larger p_ϵ^{\max} . This is shown in the left panel of Figure 5 via predictive surfaces. Also note that, for fixed ϵ , we would generally have larger τ_ϵ^2 and p_ϵ^{\max} as n increases, since that would generally result in a greater degree of insulation (10) and thus larger ω^{\max} . But details would still depend on the stochasticity of the data-generating mechanism. For deterministic responses this relationship is monotonic, so a deterministic CV (like leave-one-out) could proceed via bisection search, which would dramatically reduce the computational effort. However, we have found even that to be overkill. In all of our examples going forward we fix $\epsilon = 0.001$. For Figure 5 this results in τ_ϵ^2 values of about 20 and 30, respectively. Accordingly, our prior allows our most insulated point to “reach” a small/large probability at least as extreme as 1/1,000 and 999/1,000, possibly even more extreme when n and ω^{\max} are large. Note, this does not preclude learning something smaller via the posterior.

4.2 Simulated examples

2d Box. We first return to the two-dimensional “box” example shown in Figure 3. Due to the simplicity of this example, the results from our Monte Carlo experiment are not particularly noteworthy. We found all methods performed well for all training sizes, apart from DSVI, which achieved much lower log scores than the rest. Results from our experiment can be seen in Appendix A for those who are curious.

2d Schaffer no. 4. For a more complex 2d example, we follow Broderick and Gramacy (2011) and construct a classification problem out of a common regression example using components of partial derivatives. We borrow the Schaffer no. 4 function from the Virtual Library of Simulation Experiments (VLSE; Surjanovic and Bingham, 2013), illustrated in the top-left panel of Figure 6. The real-valued function is binarized using the x_1 -component of its gradient, where $y_i = 1$ if $\frac{\partial z}{\partial x_{i1}} > 0$, and $y_i = 0$ otherwise. The result is shown in the top-right panel, with two colors indicating the two unique classes.

Predictive performance is compared in Figure 7. For all training sizes our Vecchia-GPC consistently outperforms alternatives across both metrics. SVGP is only competitive for larger training sample sizes. However, what is apparent is the large amount of variability in performance exhibited by both SVGP and DSVI. Vecchia-GPC performance contains considerably less variability, particularly in log score, which indicates more effective UQ. Obtaining good scores is of primary importance to us. While raw accuracy (CR) is intuitive, good UQ (via LS) is our main goal.

Six-dimensional “G”. The “G” function (Marrel et al., 2009) has a jagged input-output dynamic that can be evaluated in arbitrary dimension. We borrow the VLSE form with $X \in [0, 1]^6$ and binarized real-valued output Z as $y_i = 1$ if $z_i > 1$, and $y_i = 0$ otherwise. Out-of-sample prediction results are summarized

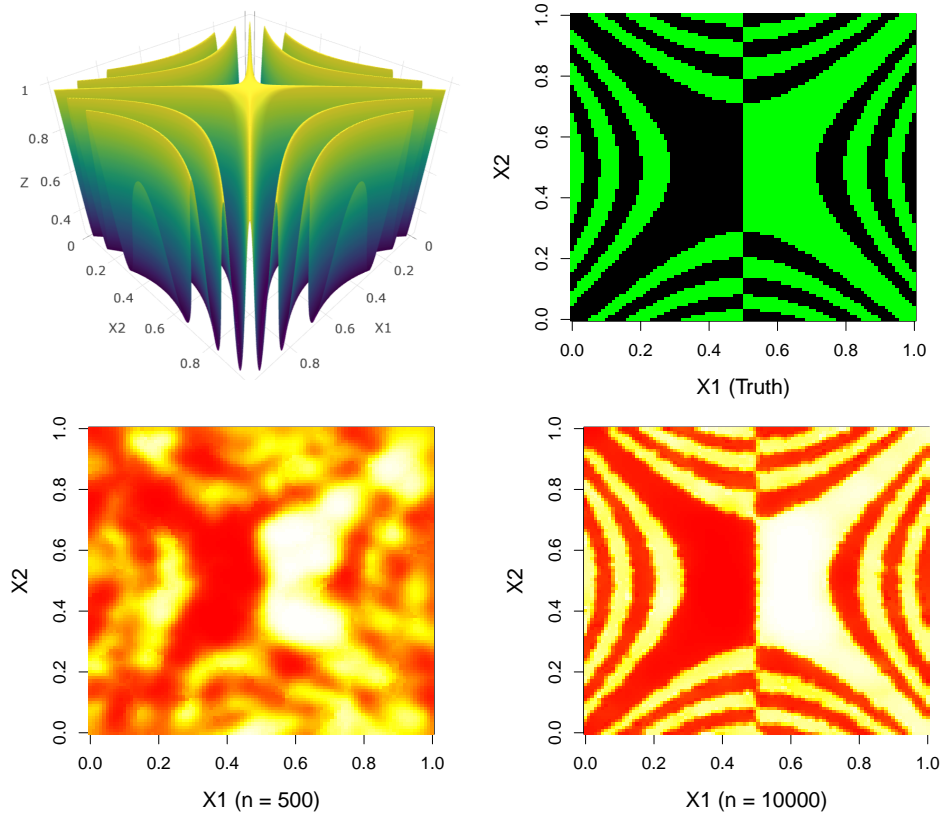


Figure 6: *Top-left*: Schaffer no. 4 function on $X \in [-2, 2]^2$. *Top-right*: Binarized version colored by class membership (black = 0, green = 1), and scaled to input space $X \in [0, 1]^2$. *Bottom*: Vecchia-GPC posterior mean predictions with $n = 500$ (*left*) and $n = 10,000$ (*right*) LHS training points, where brighter colors indicate larger success probabilities.

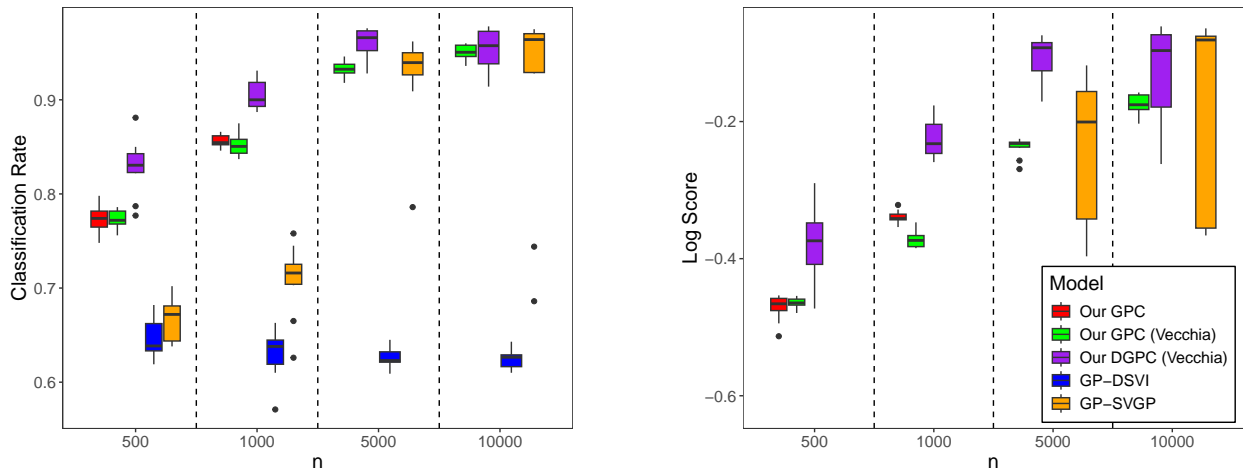


Figure 7: Schaffer function no. 4 results.

in Figure 8. Although the CR of our Vecchia-GPC is slightly lower than that of SVGP, it consistently has the highest LS across all MC iterations for smaller training sizes and exhibits less variability. SVGP

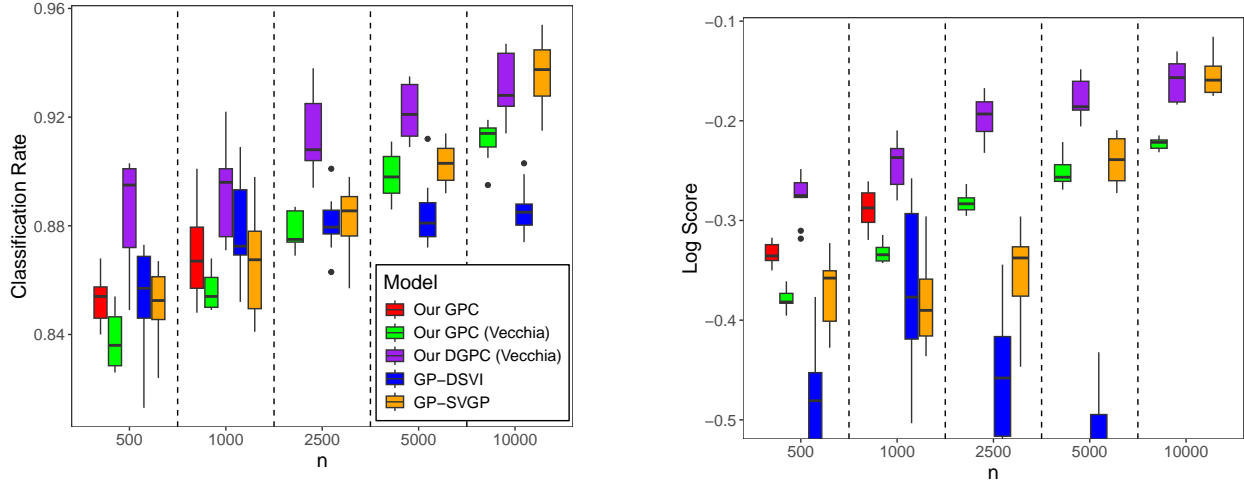


Figure 8: “G” function results.

only achieves higher LS when $n = 10,000$, and seems to perform inconsistently with less data. Our Vecchia-approximated approach doesn’t perform appreciably different than our full GPC for smaller n .

4.3 Binary black hole formation example

The COMPAS model (Riley et al., 2022) is used to study the formation of binary black holes (BBHs; Rauf et al., 2023). Eleven characteristics of two celestial bodies are given as inputs, including their respective masses and orbital separation, the magnitude and direction of the supernova natal kick vector, and others. The mass of the BBH formed – known as the “chirp mass” – is returned as output. Since BBH formation is rare (around one in ten thousand), most input configurations result “NA” instead of a valid chirp mass. So the response is of mixed type: binary (whether a BBH formed or not) and numeric (if one formed, what is its mass). More formally, if $x \in [0, 1]^{11}$ represents coded inputs, and $m(x)$ is the output COMPAS, then $y(x) = \mathbb{I}(m(x) \in \mathbb{R}^+)$ indicates BBH formation. Figure 9 illustrates the relationship between some of the

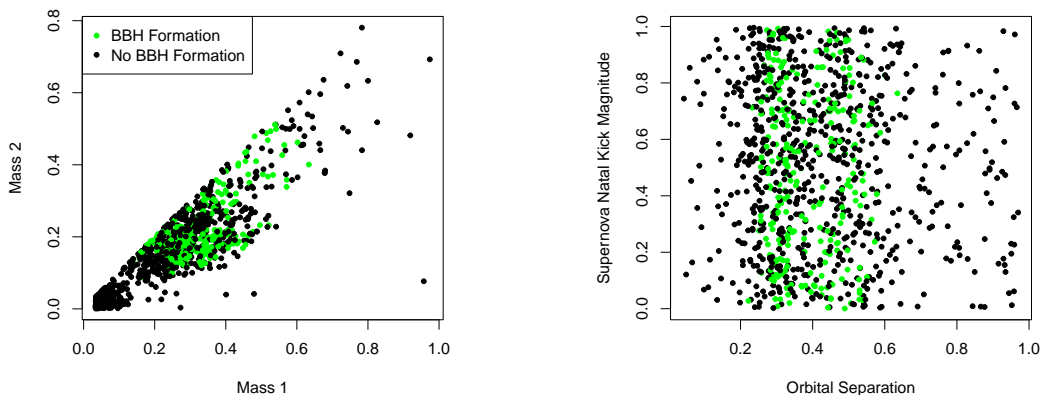


Figure 9: COMPAS simulations projected onto two pairs of inputs. Green dots indicate BBH formations.

inputs and BBH formation. The left panel projects a subset of evaluations collected by Lin et al. (2021) onto the two celestial mass inputs, where the first object denotes the more massive of the two. The right

panel projects the same data onto the orbital separation and supernova natal kick magnitudes. Observe in both plots how BBH formations occur in relatively small sub-regions of the input space. For instance, orbital separation values outside of $[0.2, 0.6]$ or greater than 0.6 almost never yield a BBH.

We use simulations from the COMPAS provided by [Lin et al. \(2021\)](#), which involved using adaptive importance sampling to boost the percentage of BBH formations to around 27%. We randomly subsampled these data into ten unique training sets of size $n = 10,000$, then fit GP-based classifiers [Section 4.1] for 1,000 testing locations randomly drawn from the remaining samples. Results are shown in Figure 10. In

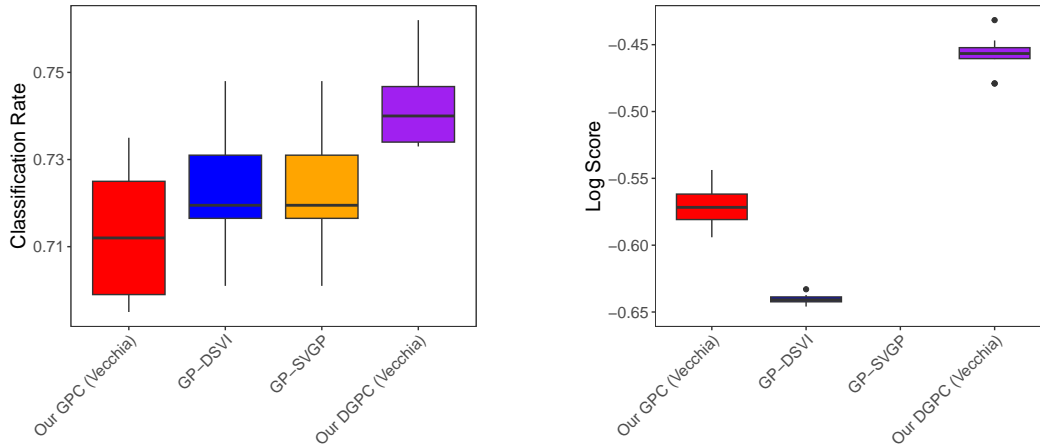


Figure 10: BBH comparison. SVGP’s LSs are out-of-frame, being well below the other methods.

terms of pure accuracy (CR), all three models perform similarly. While DSVI and SVGP achieve slightly better CR, our GPC has the highest median CR and has less variability across the ten runs. What’s more striking is the comparison on LS. SVGP’s are so poor, they fall below the y -axis and are not shown. Our Vecchia GPC obtained the best LS in all ten of the MC instances.

5 Deep Gaussian process classification

Most GPs make an assumption of *stationarity*; i.e., that modeling – via the MVN covariance structure – depends only on relative input distance, not input position. A nonstationary regression surface (i.e., with real-valued outputs) is easy to describe as having disparate regimes in the input space, say one region where outputs are wiggly and another that’s changing more gradually. Nonstationarity in classification is more subtle. The deterministic nature of simulators like the BBH, or any of the synthetic examples we have explored so far, means transitions between output classes are always abrupt.

To illustrate the nuances of nonstationarity in a classification setting, consider the Schaffer function from Section 4.2, re-depicted in the left panel of Figure 11. Two horizontal slices are shown in the middle and right panels, in red and blue, respectively. Notice how transitions are more evenly spaced in the first slice than the second. Broadly, labels change less rapidly in the middle of the space than near the edges/corners. Since the behavior of the response is affected by both position and relative distance, our GP classifier would benefit from additional nonstationary flexibility.

5.1 DGPC methodology and implementation

For real-valued, regression GPs, there are many approaches to relaxing stationarity, including process convolutions ([Higdon, 1998](#)) and spectral kernels ([Remes et al., 2017](#)). For a comprehensive overview, see

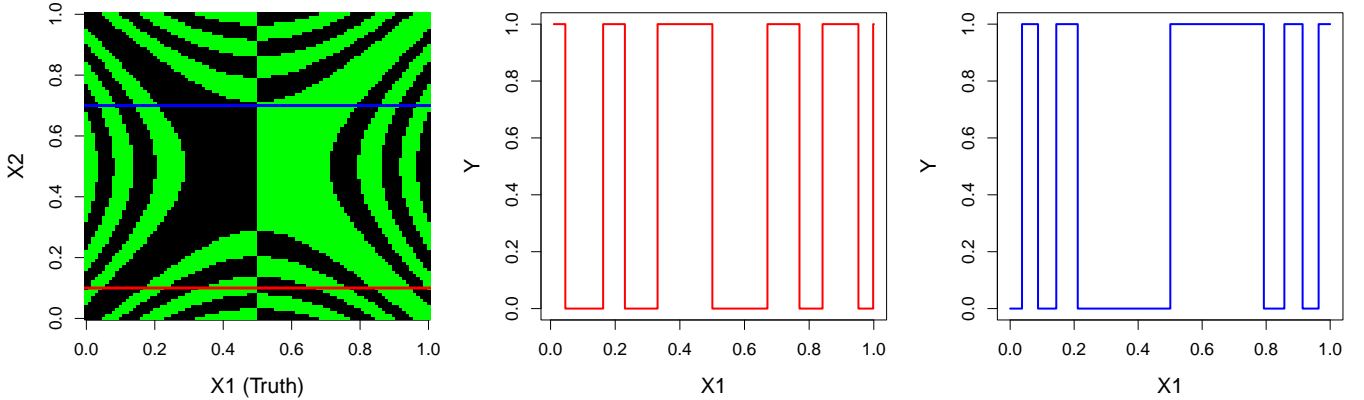


Figure 11: 2d Schaffer function (*left*) with slices along $x_2 = 0.1$ (*middle*, red) and $x_2 = 0.7$ (*right*, blue).

Booth et al. (2024). One increasingly popular strategy was formerly known as *input warping* (Sampson and Guttorp, 1992; Schmidt and O’Hagan, 2003). The idea is to adjust the inputs so that stationary modeling is appropriate. Sampson and Guttorp saw this as a pre-processing step, whereas Schmidt and O’Hagan considered joint inference for *latent*, warped inputs ($X \rightarrow W$) and downstream input–output ($W \rightarrow Z$) modeling. Placing a GP prior on both mappings creates a functional composition much like a two-layer neural network (NNs), but with GPs. Piggybacking off of buzz for deep NNs, Damianou and Lawrence (2012) rebranded the idea as deep GPs (DGPs), entertaining further (deeper) layers of composition.

Damianou and Lawrence’s main contribution involved modernizing inference for the latent, warped “layers”, W . Schmidt and O’Hagan’s Metropolis approach suffers the same limitations outlined earlier [Section 2.2] for latent Z -variables in a classification context, limiting applicability to small data sizes. Damianou and Lawrence’s VI/IP allowed for much larger n , in neat symmetry to the situation we described earlier for classification with GPs: cumbersome sampling replaced by optimization and approximation. But like in that setting, computational gains come at the expense of fidelity and UQ.

Sauer et al. (2022b) recognized that ESS is ideal for fully Bayesian, posterior integration of latent warping variables. With the right inferential mechanism (ESS), and covariance approximation (Vecchia), two-layer DGPs were sufficient for modeling nonstationary simulation dynamics (Sauer et al., 2022a). We appropriated many of those ideas for classification in Section 3 in a one-layer, shallow GPC context. Here we chain the two together, bolting an additional latent Bernoulli layer onto a DGP regression for classification (DGPC). This is easy to say, but hard to do, which may be why it has yet to be done.

Let $W \in \mathbb{R}^{n \times d}$ represent a d -dimensional warping layer situated between $X \in \mathbb{R}^{n \times d}$ and logistic latent $Z \in \mathbb{R}^n$ variables. While W can be of any column dimension, it is perhaps most intuitive to match with X . Sauer et al. (2022b) showed that using a lower dimensional warping, providing an *autoencoder*-like effect by analogy to DNNs (Kingma and Welling, 2022), may have deleterious performance for computer experiments. The architecture of our model is diagrammed and detailed hierarchically in Figure 12. Observe the solid red arrows from X to the coordinates of W ; each represents a separate, independent GP (see the equation in red to the right). These collectively map X to a warped version of itself ($W = [W_1, W_2, \dots, W_d]$), which is fed as input to the latent GP for Z (green arrow), then logistically-transformed to a success probability for Y (blue dotted line). We introduce subscripts θ_z and $(\theta_{w_1}, \dots, \theta_{w_d})$ to denote the covariance matrices constructed with independent lengthscales for Z and each coordinate of W , respectively.

Algorithm 3 outlines our Gibbs procedure for DGPC. Samples for each θ_{w_j} are generated through MH via the MVN likelihood $\mathcal{L}(W_j|X, \theta_{w_j})$. Posterior sampling for each coordinate of W follows ESS (Sauer

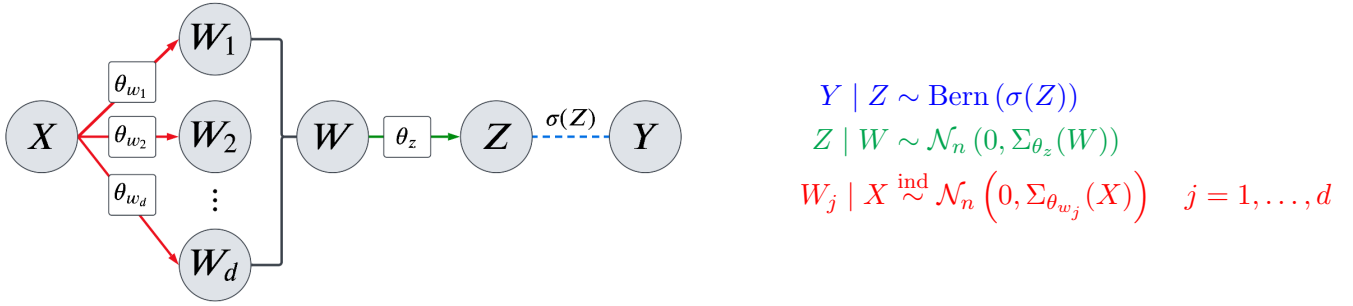


Figure 12: *Left*: Diagram of two-layer DGPC. Each arrow corresponds to a separate GP. *Right*: DGPC model hierarchy, color-coded to match components of the diagram.

et al., 2022b). Specifically, take $W_j \sim \mathcal{N}_n(0, \Sigma_{\theta_{w_j}}(X))$, then convolve with $W_j^{(t)}$ via a random angle γ to propose W_j^* [Alg. 1]. Acceptance is based on the likelihood ratio $\mathcal{L}(Z | W^*, \theta_z) / \mathcal{L}(Z | W^{(t)}, \theta_z)$, with only the j^{th} column of W^* and $W^{(t)}$ differing at a time. Finally, posterior samples of Z can be obtained by substituting $W^{(t)}$ in place of X in the ESS procedure outlined in Alg. 1. Altogether, Alg. 3 is similar to Alg. 2 with additional loops for W_j and its lengthscale(s).

Algorithm 3: Gibbs sampling procedure for two-layer DGPC estimation.

```

Initialize  $\theta_{w_1}^{(1)}, \dots, \theta_{w_d}^{(1)}, \theta_z^{(1)}, W^{(1)}, Z^{(1)}$ 
for  $t = 2, \dots, T$  do
  for  $j = 1, \dots, d$  do
     $\theta_{w_j}^{(t)} \sim \pi(\theta_{w_j} | X, W_j^{(t-1)})$  // MH via  $\mathcal{L}(W_j | X, \theta_{w_j})$ 
     $W_j^{(t)} \sim \pi(W_j | X, Z^{(t-1)}, \theta_{w_j}^{(t)})$  // ESS via  $\mathcal{L}(W_j | X, \theta_{w_j}), \mathcal{L}(Z^{(t-1)} | W, \theta_z)$ 
   $\theta_z^{(t)} \sim \pi(\theta_z | W^{(t)}, Z^{(t-1)})$  // MH via  $\mathcal{L}(Z | W, \theta_z)$ ; like Alg. 2 with  $W$  for  $X$ 
   $Z^{(t)} \sim \pi(Z | W^{(t)}, Y, \theta_z^{(t)})$  // ESS via  $\mathcal{L}(Z | W, \theta_z), \mathcal{L}(Y | Z)$ ; like Alg. 2 with  $W$  for  $X$ 

```

Predictive quantities for new inputs \mathcal{X} involve additional MC sampling like with the ordinary GPC. Posterior draws for \mathcal{Z} require feeding samples from Alg. 3 through a cascade of kriging equations (3). For example, take $\mathcal{W}_j^{(t)}(\mathcal{X}) | X, W_j^{(t)}$ by replacing Y with $W_j^{(t)}$ and using $\theta_{w_j}^{(t)}$ within each $\Sigma(\cdot)$. Combine these samples for all j to form $\mathcal{W}^{(t)} = [\mathcal{W}_1^{(t)}, \dots, \mathcal{W}_d^{(t)}]$. Then form $\mathcal{Z}^{(t)}(\mathcal{W}^{(t)}) | W^{(t)}, Z^{(t)}$ in a similar fashion. From there we can approximate the mean and variance of $p_y(x)$ for each $x \in \mathcal{X}$ just as for ordinary GPC (8). Introducing d additional GPs compounds the computational burden for training and prediction, especially when d is large like for the BBH. Yet the same Vecchia approximations are applicable, both for inference and prediction. Implementation is similar to that of Section 4, via separate randomized orderings for each of the $d + 1$ GPs. The entire procedure remains cubic in the conditioning set size, m .

5.2 DGPC performance comparison

First consider a two-layer deep GPC on the simulated examples from Section 4.2. Figure 13 demonstrates improved predictive resolution for the 2d Schaffer no. 4 example. The left panel shows the posterior mean success probability surface from our ordinary GPC trained on an LHS design of size $n = 1,000$; the

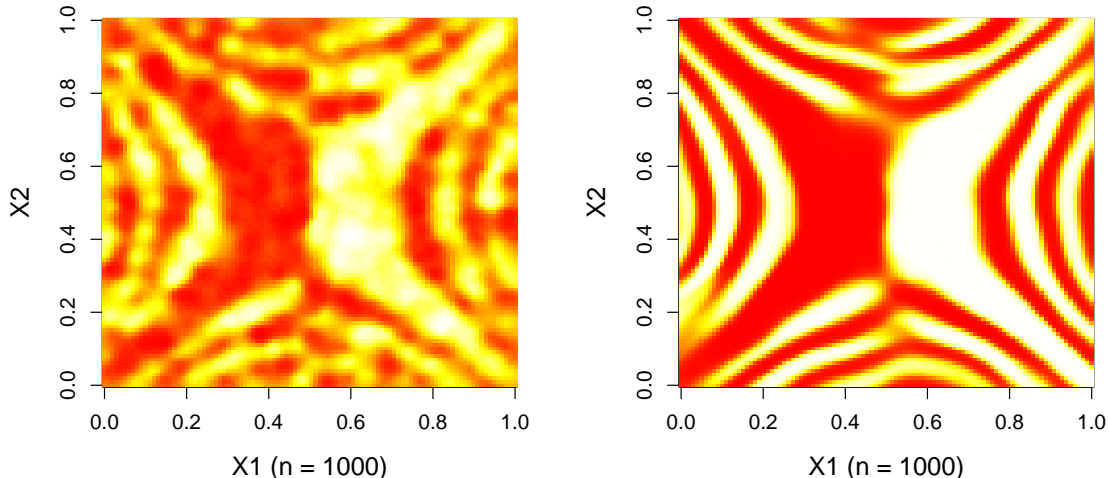


Figure 13: Vecchia GPC (*left*) and DGPC (*right*) on 2d Schaffer no. 4 with the identical training points.

right panel shows a two-layer DGPC on the same data. Notice how the DGPC provides sharper transitions between labels, especially at the edges/corners. Moreover, it furnishes more confident probability estimates in regions of a single class, as seen by the brighter colors in the middle.

Out-of sample performance for DGPC is provided by the purple boxplots contained in Figures 7 and 8, for the Schaffer and “G” functions, respectively. In both cases, the additional depth of the DGPC leads to a significant improvement in accuracy (CR) and UQ (LS), especially for smaller n . With larger n , additional depth provides diminishing returns. Ultimately, both GP and DGP are universal approximators. DGPC performance on BBH classification is provided by the purple boxplots in Figure 10. It provides both the highest median classification accuracy and the most effective UQ (as indicated by high LS).

6 Discussion

We have deployed the Vecchia approximation to make fully Bayesian GP classification (GPC) feasible in large-data settings. By speeding up matrix decomposition through sparsity-inducing approximations, which fit naturally into the previously intractable elliptical slice sampling framework for latent GP classification, we have allowed for GPC training in large data settings without sacrificing full uncertainty quantification (UQ). This has led to improved accuracy and UQ, as demonstrated on a suite of benchmark problems and a real binary black hole simulator. Additionally, we have shown how additional input-warping layers could be accommodated similarly, resulting in a deep GP classifier, for nonstationary classification.

While our work in this paper focuses on binary classification, the extension to more than two classes is straightforward (Rasmussen and Williams, 2006). Inference for a response with K classes can be performed by expanding Z to $K - 1$ independent GP layers (Seeger and Jordan, 2004). Let $Z_k \sim \mathcal{N}(0, \Sigma_k(X))$ for $k = 1, \dots, K - 1$, where each $\Sigma_k(X)$ contains its own covariance hyperparameters. The *generalized* logistic function transforms this layer into valid probabilities: $\sigma(z_{ik}) = \frac{e^{-z_{ik}}}{1 + \sum_{\ell=1}^{K-1} e^{-z_{i\ell}}}$, where z_{ik} represents the i^{th} entry of the k^{th} layer of Z . When $K = 2$ this function simplifies to the sigmoid inverse-link function seen in Section 2.2. Our publicly available implementation in \mathbb{R}^1 supports multiclass classification.

¹bitbucket.org/gramacylab/deepgp_class

Previous research on COMPAS/BBH has focused on regression for predicting chirp mass. [Lin et al. \(2021\)](#) propose a local classification GP to predict BBH formation where inputs predicted as non-NA feed into a chirp mass surrogate. However, their point-estimation approach may undercut on UQ. Combining our approach with a fully Bayesian regression GP may be an interesting avenue for further research. An alternative model, recently proposed by [Yazdi et al. \(2024\)](#), skips the classification step to directly model NA values as zero with a DGP. It would be of interest to contrast these two approaches.

References

- Abrahamsen, P. (1997). “A review of Gaussian random fields and correlation functions.” Norsk Regnesentral/Norwegian Computing Center Oslo, https://www.nr.no/directdownload/917_Rapport.pdf.
- Albert, J. H. and Chib, S. (1993). “Bayesian analysis of binary and polychotomous response data.” *Journal of the American statistical Association*, 88, 422, 669–679.
- Banerjee, A., Dunson, D. B., and Tokdar, S. T. (2013). “Efficient Gaussian process regression for large datasets.” *Biometrika*, 100, 1, 75–89.
- Bates, D., Maechler, M., Jagan, M., et al. (2010). “Matrix: Sparse and dense matrix classes and methods.” *R package version 0.999375-43*, URL <http://cran.r-project.org/package=Matrix>.
- Binois, M., Gramacy, R. B., and Ludkovski, M. (2018). “Practical heteroscedastic Gaussian process modeling for large simulation experiments.” *Journal of Computational and Graphical Statistics*, 27, 4, 808–821.
- Booth, A. S., Cooper, A., and Gramacy, R. B. (2024). “Nonstationary Gaussian process surrogates.” *arXiv preprint arXiv:2305.19242*.
- Broderick, T. and Gramacy, R. B. (2011). “Classification and categorical inputs with treed Gaussian process models.” *Journal of classification*, 28, 2, 244–270.
- Cao, J., Kang, M., Jimenez, F., Sang, H., Schäfer, F., and Katzfuss, M. (2023). “Variational Sparse Inverse Cholesky Approximation for Latent Gaussian Processes via Double Kullback-Leibler Minimization.”
- Cole, D. A., Christianson, R. B., and Gramacy, R. B. (2021). “Locally induced Gaussian processes for large-scale simulation experiments.” *Statistics and Computing*, 31, 3, 1–21.
- Damianou, A. C. and Lawrence, N. D. (2012). “Deep Gaussian Processes.” *Proceedings of Machine Learning Research*.
- Damianou, A. C., Titsias, M. K., Gr, M., Lawrence, N. D., and Storkey, A. (2016). “Variational Inference for Latent Variables and Uncertain Inputs in Gaussian Processes.”
- Datta, A. (2021). “Sparse Cholesky matrices in spatial statistics.” *arXiv preprint arXiv:2102.13299*.
- Datta, A., Banerjee, S., Finley, A. O., and Gelfand, A. E. (2016). “Hierarchical nearest-neighbor Gaussian process models for large geostatistical datasets.” *Journal of the American Statistical Association*, 111, 514, 800–812.
- Dunlop, M. M., Girolami, M. A., Stuart, A. M., and Teckentrup, A. L. (2018). “How deep are deep Gaussian processes?” *Journal of Machine Learning Research*, 19, 54, 1–46.

- Dutordoir, V., Salimbeni, H., Hambro, E., McLeod, J., Leibfried, F., Artemev, A., van der Wilk, M., Deisenroth, M. P., Hensman, J., and John, S. (2021). “GPflux: A library for Deep Gaussian Processes.” *arXiv:2104.05674*.
- Eddelbuettel, D. and Sanderson, C. (2014). “RcppArmadillo: Accelerating R with high-performance C++ linear algebra.” *Computational statistics & data analysis*, 71, 1054–1063.
- Emery, X. (2009). “The kriging update equations and their application to the selection of neighboring data.” *Computational Geosciences*, 13, 3, 269–280.
- Frühwirth-Schnatter, S. and Frühwirth, R. (2010). “Data augmentation and MCMC for binary and multinomial logit models.” *Statistical modelling and regression structures: Festschrift in honour of Ludwig Fahrmeir*, 111–132.
- Gelman, A., Carlin, J. B., Stern, H. S., and Rubin, D. B. (1995). *Bayesian data analysis*. Chapman and Hall/CRC.
- Gneiting, T. and Raftery, A. (2007). “Strictly proper scoring rules, prediction, and estimation.” *Journal of the American Statistical Association*, 102, 477, 359–378.
- Gramacy, R. B. (2020). *Surrogates: Gaussian Process Modeling, Design and Optimization for the Applied Sciences*. Boca Raton, Florida: Chapman Hall/CRC. <http://bobby.gramacy.com/surrogates/>.
- Gramacy, R. B. and Apley, D. W. (2015). “Local Gaussian process approximation for large computer experiments.” *Journal of Computational and Graphical Statistics*, 24, 2, 561–578.
- Gramacy, R. B. and Lee, H. K. (2012). “Cases for the nugget in modeling computer experiments.” *Statistics and Computing*, 22, 713–722.
- Gramacy, R. B. and Polson, N. G. (2011). “Particle Learning of Gaussian Process Models for Sequential Design and Optimization.” *Journal of Computational and Graphical Statistics*, 20, 1, 102–118.
- Hastings, W. K. (1970). “Monte Carlo sampling methods using Markov chains and their applications.” *Biometrika*.
- Hensman, J., Matthews, A., and Ghahramani, Z. (2015). “Scalable variational Gaussian process classification.” In *Artificial Intelligence and Statistics*, 351–360. PMLR.
- Higdon, D. (1998). “A process-convolution approach to modelling temperatures in the North Atlantic Ocean.” *Environmental and Ecological Statistics*, 5, 173–190.
- Jin, H. and Yin, G. (2021). “Unit information prior for adaptive information borrowing from multiple historical datasets.” *Statistics in Medicine*, 40, 25, 5657–5672.
- Jones, D., Schonlau, M., and Welch, W. (1998). “Efficient global optimization of expensive black-box functions.” *Journal of Global Optimization*, 13, 4, 455–492.
- Katzfuss, M. and Guinness, J. (2021). “A General Framework for Vecchia Approximations of Gaussian Processes.” *Statistical Science*, 36, 124–141.
- Katzfuss, M., Guinness, J., Gong, W., and Zilber, D. (2020). “Vecchia approximations of Gaussian-process predictions.” *Journal of Agricultural, Biological and Environmental Statistics*, 25, 383–414.

- Katzfuss, M., Guinness, J., and Lawrence, E. (2022). “Scaled Vecchia approximation for fast computer-model emulation.” *SIAM/ASA Journal on Uncertainty Quantification*, 10, 2, 537–554.
- Kennedy, M. and O’Hagan, A. (2001). “Bayesian calibration of computer models.” *Journal of the Royal Statistical Society: Series B (Statistical Methodology)*, 63, 3, 425–464.
- Kingma, D. P. and Welling, M. (2022). “Auto-Encoding Variational Bayes.”
- Lázaro-Gredilla, M., Quinonero-Candela, J., Rasmussen, C. E., and Figueiras-Vidal, A. R. (2010). “Sparse spectrum Gaussian process regression.” *The Journal of Machine Learning Research*, 11, 1865–1881.
- Lin, L., Bingham, D., Broekgaarden, F., and Mandel, I. (2021). “Uncertainty Quantification of a Computer Model for Binary Black Hole Formation.” *Annals of Applied Statistics*. Real world example of gp’s for classification for purpose of classifying types of black holes.
- Marrel, A., Iooss, B., Laurent, B., and Roustant, O. (2009). “Calculations of Sobol indices for the Gaussian process metamodel.” *Reliability Engineering & System Safety*, 94, 3, 742–751.
- Matheron, G. (1963). “Principles of geostatistics.” *Economic geology*, 58, 8, 1246–1266.
- Matthews, A. G. d. G., van der Wilk, M., Nickson, T., Fujii, K., Boukouvalas, A., León-Villagrà, P., Ghahramani, Z., and Hensman, J. (2017). “GPflow: A Gaussian process library using TensorFlow.” *Journal of Machine Learning Research*, 18, 40, 1–6.
- McCullagh, P. and Nelder, J. A. (1989). *Generalized Linear Models*. London: Chapman & Hall / CRC.
- McKay, M. D., Beckman, R. J., and Conover, W. J. (1979). “A comparison of three methods for selecting values of input variables in the analysis of output from a computer code.” *Technometrics*, 21, 2, 239–245.
- Melkumyan, A. and Ramos, F. T. (2009). “A sparse covariance function for exact Gaussian process inference in large datasets.” In *Twenty-first international joint conference on artificial intelligence*.
- Minka, T. P. (2001). “A family of algorithms for approximate Bayesian inference.” Ph.D. thesis, Massachusetts Institute of Technology.
- Morris, M. D., Mitchell, T. J., and Ylvisaker, D. (1993). “Bayesian Design and Analysis of Computer Experiments: Use of Derivatives in Surface Prediction.” *Technometrics*, 35, 3, 243–255.
- Murray, I., Prescott, R., David, A., and Mackay, J. C. (2010). “Elliptical slice sampling.”
- Neal, R. (1998). “Regression and classification using Gaussian process priors.” *Bayesian statistics*, 6, 475.
- Neal, R. M. (2003). “Slice sampling.” *The annals of statistics*, 31, 3, 705–767.
- Quinonero-Candela, J. and Rasmussen, C. E. (2005). “A unifying view of sparse approximate Gaussian process regression.” *The Journal of Machine Learning Research*, 6, 1939–1959.
- Quiñonero, J., Quiñonero-Candela, Q., Rasmussen, C. E., and De, C. M. (2005). “A Unifying View of Sparse Approximate Gaussian Process Regression.” *Inducing points*.
- Rasmussen, C. E. and Williams, C. K. I. (2006). *Gaussian processes for machine learning*. MIT Press.

- Rauf, L., Howlett, C., Davis, T. M., and Lagos, C. D. (2023). “Exploring binary black hole mergers and host galaxies with shark and COMPAS.” *Monthly Notices of the Royal Astronomical Society*, 523, 4, 5719–5737.
- Remes, S., Heinonen, M., and Kaski, S. (2017). “Non-stationary spectral kernels.” *Advances in neural information processing systems*, 30.
- Riley, J., Agrawal, P., Barrett, J. W., Boyett, K. N. K., Broekgaarden, F. S., Chattopadhyay, D., Gaebel, S. M., Gittins, F., Hirai, R., Howitt, G., Justham, S., Khandelwal, L., Kummer, F., Lau, M. Y. M., Mandel, I., de Mink, S. E., Neijssel, C., Riley, T., van Son, L., Stevenson, S., Vigna-Gómez, A., Vinciguerra, S., Wagg, T., Willcox, R., and Team Compas (2022). “Rapid Stellar and Binary Population Synthesis with COMPAS.” *The Astrophysical Journal*, 258, 2, 34.
- Robert, C. P., Casella, G., and Casella, G. (1999). *Monte Carlo statistical methods*, vol. 2. Springer.
- Salimbeni, H. and Deisenroth, M. (2017). “Doubly Stochastic Variational Inference for Deep Gaussian Processes.” *31st Conference on Neural Information Processing Systems*. Dsvi.
- Sampson, P. D. and Guttorp, P. (1992). “Nonparametric estimation of nonstationary spatial covariance structure.” *Journal of the American Statistical Association*, 87, 417, 108–119.
- Santner, T., Williams, B., and Notz, W. (2018). *The Design and Analysis of Computer Experiments, Second Edition*. New York, NY: Springer-Verlag.
- Sauer, A., Cooper, A., and Gramacy, R. B. (2022a). “Vecchia-approximated deep Gaussian processes for computer experiments.” *Journal of Computational and Graphical Statistics*, 32, 3, 824–837.
- Sauer, A., Gramacy, R. B., and Higdon, D. (2022b). “Active learning for deep Gaussian process surrogates.” *Technometrics*, 65, 1, 4–18.
- Schmidt, A. M. and O’Hagan, A. (2003). “Bayesian inference for non-stationary spatial covariance structure via spatial deformations.” *Journal of the Royal Statistical Society Series B: Statistical Methodology*, 65, 3, 743–758.
- Seeger, M. and Jordan, M. (2004). “Sparse Gaussian process classification with multiple classes.” Tech. rep., Department of Statistics, University of Berkeley, CA.
- Snelson, E. and Ghahramani, Z. (2006). “Sparse Gaussian Processes using Pseudo-inputs.” *Advances in Neural Information Processing Systems 18*, 1257–1264.
- Stein, M. L., Chi, Z., and Welty, L. J. (2004). “Approximating likelihoods for large spatial data sets.” *Journal of the Royal Statistical Society Series B: Statistical Methodology*, 66, 2, 275–296.
- Stroud, J. R., Stein, M. L., and Lysen, S. (2017). “Bayesian and maximum likelihood estimation for Gaussian processes on an incomplete lattice.” *Journal of computational and Graphical Statistics*, 26, 1, 108–120.
- Surjanovic, S. and Bingham, D. (2013). “Virtual Library of Simulation Experiments: Test Functions and Datasets.” Retrieved May 21, 2024, from <http://www.sfu.ca/~ssurjano>.

- Titsias, M. (2009). “Variational Learning of Inducing Variables in Sparse Gaussian Processes.” In *Proceedings of the Twelfth International Conference on Artificial Intelligence and Statistics*, eds. D. van Dyk and M. Welling, vol. 5 of *Proceedings of Machine Learning Research*, 567–574. Hilton Clearwater Beach Resort, Clearwater Beach, Florida USA: PMLR.
- Vecchia, A. (1988). “Estimation and model identification for continuous spatial processes.” *Journal of the Royal Statistical Society: Series B (Methodological)*, 50, 2, 297–312.
- Williams, C. K. and Barber, D. (1998). “Bayesian classification with Gaussian processes.” *IEEE Transactions on pattern analysis and machine intelligence*, 20, 12, 1342–1351.
- Wu, L., Pleiss, G., and Cunningham, J. (2022). “Variational Nearest Neighbor Gaussian Processes.” *arXiv preprint arXiv:2202.01694*.
- Yazdi, F., Bingham, D., and Williamson, D. (2024). “Deep Gaussian Process Emulation and Uncertainty Quantification for Large Computer Experiments.”
- Zilber, D. and Katzfuss, M. (2021). “Vecchia–Laplace approximations of generalized Gaussian processes for big non-Gaussian spatial data.” *Computational Statistics & Data Analysis*, 153, 107081.

A 2d box results

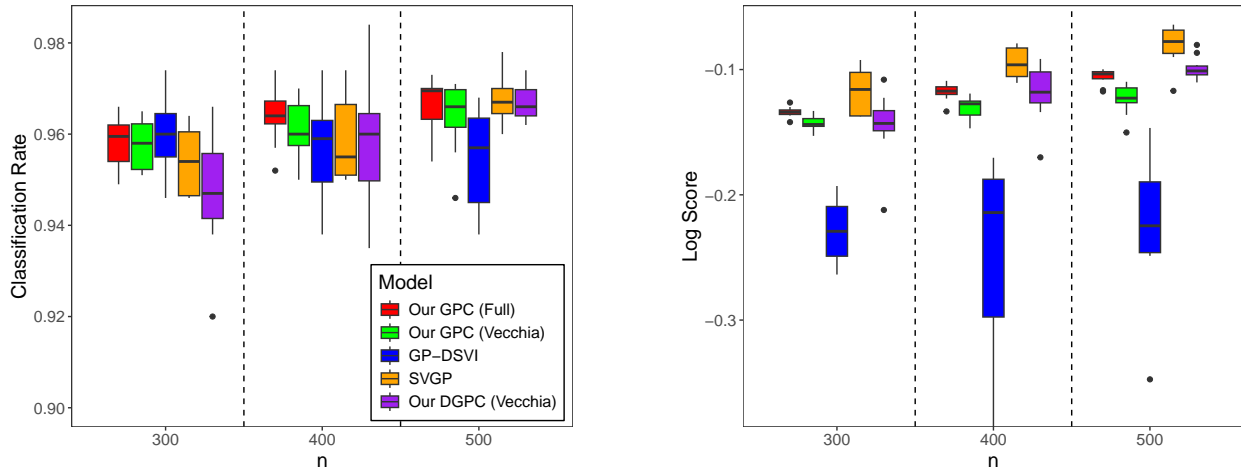


Figure 14: Two-dimensional “box” results. Some negative outliers for DSVI’s log score are cut off from the plot to make the rest of the boxplots more readable.

Results for the two-dimensional box example are presented via boxplots in Figure 14. The full GPC slightly outperforms the Vecchia-approximated GPC (albeit at higher computational expense). DSVI performs poorly across the board. SVGP performs slightly better on average for training sizes of $n = 500$, but has slightly larger variance than our method in both classification rate and log score. Vecchia-DGPC only outperforms our ordinary GPC when $n = 500$, indicating more data is needed for the benefits of adding deepness to be readily apparent. Note, a few lower outliers from DSVI in both classification rate and log score are not shown for plot scaling purposes to highlight the performance of the rest of the methods.